Arabian Journal for Science and Engineering
https://doi.org/10.1007/s13369-025-10604-0

RESEARCH ARTICLE-CHEMISTRY

Synthesis of a Novel Bio-adsorbent Composite Combining Chitosan Powder and *Opuntia ficus-indica* Cladodes: Characterization and Application for Heavy Metal Removal from Water

Abdelhamid Mili[1] · Slimane Kadouche[3] · Juliette Vievard[2] · Ferhat Mourad[1] · Radia Tafer[4] · Christine Devouge-Boyer[2] · Abdelaziz Boulkamh[4] · Mélanie Mignot[2]

Received: 30 April 2025 / Accepted: 26 August 2025
© King Fahd University of Petroleum & Minerals 2025

Abstract

Rapid urbanization and industrialization have led to significant pollution of surface and groundwater by heavy metals, posing risks to ecosystems and human health. In this study, Opuntia ficus-indica (OFI) and chitosan (CS) were combined to enhance the adsorption properties of both materials. The resulting OFI/CS composites, at 1:1 and 1:2 mass ratios, were characterized by FTIR, SEM/EDX, and elemental analysis. The adsorption efficiencies of the materials were tested for the removal from water of Pb(II), Cu(II), Ni(II) and Cd(II) in a multi-heavy metal system, across a concentration range of [10–100] mg/L. The effects of pH, contact time, and initial adsorbent concentration were investigated to evaluate the adsorbents' capacities and kinetics. Experimental findings showed that the OFI/CS 1:1 composite exhibited high removal efficiencies, exceeding 90% for Pb(II) and Cu(II), and over 40% for Ni(II) and Cd(II), after 180 min of contact, using a bio-adsorbent dosage of 5 g/L and an initial individual heavy metals concentration of 100 mg/L. Among the kinetic models tested, the Elovich was the most suitable, indicating chemisorption. Regarding the isotherms, the Langmuir model provided the best fit for Pb(II) and Cu(II), while the Freundlich and Dubinin–Radushkevich (D–R) models better described the behavior of Ni(II) and Cd(II). The highest adsorption capacity was obtained with the OFI/CS 1:1 composite, reaching 102 mg/g for lead and a cumulative value of 183 mg/g. These results highlight the promising potential of OFI/CS composites, particularly the 1:1 ratio, for the effective removal of heavy metals from contaminated water.

Keywords Bio-adsorption · Heavy metals removal · Opuntia ficus-indica · Chitosan · Composite · Water decontamination

1 Introduction

Rapid urbanization and industrialization have led to one of the most pressing issues of our time: water scarcity. It has become increasingly urgent to treat industrial wastewater, such as that generated from textile manufacturing, dyeing, and battery production, which causes serious environmental damage [1]. Heavy metal contamination of surface and groundwater has emerged as a major global environmental concern. This pollution negatively affects ecosystems, human health, and other life forms due to the bioaccumulation of heavy metals in food chains [2]. Heavy metals can enter the human body through various pathways, including the ingestion of contaminated food and water, potentially causing symptoms such as vomiting, nasal irritation, and nervous system damage. Although trace amounts of certain metals like zinc, iron, and manganese are essential for physiological functions, higher concentrations can be toxic [3]. Heavy metal pollution stems from intensified anthropogenic activities such as mining, metal foundries, industrial processing, oil and gas extraction, wastewater discharge, road traffic, and landfills.

✉ Slimane Kadouche
slimane.kadouche@ummto.dz

1 Laboratory of Materials and Sustainable Development (LMDD), Faculty of Exact Sciences, University of Bouira, 10000 Bouira, Algeria

2 CARMeN UMR 6064, INC3M FR 3038, CNRS, INSA Rouen Normandie, Univ Rouen Normandie, Normandie Univ, F-76000 Rouen, France

3 Laboratory of Applied Chemistry and Chemical Engineering (LCAGC), Faculty of Sciences, UMMTO, 15000 Tizi Ouzou, Algeria

4 Laboratory of Innovative Environmental Preservation Techniques, Department of Chemistry, Constantine 1 University, Constantine, Algeria

Published online: 16 September 2025

Recent studies have focused on innovative heavy metal remediation techniques, emphasizing various strategies to reduce environmental contamination. Yang et al. [4] investigated the use of biochar derived from bamboo and rice straw in contaminated paddy soil, showing that its application significantly reduced the extractability of metals such as Cd(II), Cu(II), Pb(II), and Zn(II), while enhancing soil enzyme activity. Zhang et al. [5] synthesized hybrid nanoparticles using carboxymethylated lignin, demonstrating rapid and highly efficient adsorption of Pb(II) and Cu(II) from water, with adsorption capacities of 150 and 70.7 mg/g, respectively, reaching equilibrium in less than 30 min. Mubashar et al. [6] examined the combined use of the microalga *Chlorella vulgaris* and *Enterobacter* sp. MN17 for removing heavy metals and reducing chemical oxygen demand (COD) in textile wastewater. They reported substantial reductions in metal concentrations, up to 93% for Cd(II), 79% for Cr(VI) and Pb(II), and 72% for Cu(II), highlighting the potential of algae-bacteria consortia in efficient bioremediation. These findings underscore the importance of bio-based and hybrid materials for environmental protection.

Biochar is one of the most widely studied biomaterials for pollution mitigation; however, it faces several challenges. Its properties vary significantly depending on feedstock type and pyrolysis conditions, which can greatly affect its adsorption capacity and overall performance. Additionally, biochar may have limited long-term stability, possibly resulting in contaminant leaching back into soils. Moreover, producing high-quality biochar can be costly and energy-intensive. These limitations underscore the need for more effective, economical, and sustainable alternatives [7].

A range of techniques currently exists to treat water pollution from both organic and inorganic sources. These include physical methods such as adsorption, bioadsorption, ion exchange, membrane filtration, and coagulation/precipitation; chemical methods such as photocatalysis and electrochemistry; and biological methods [8–10]. Bioadsorption has recently gained attention as a promising water treatment technique due to its low cost and ease of use, particularly when employing abundant natural resources [11].

Opuntia ficus-indica, commonly known as prickly pear, belongs to the cactus family (Cactaceae), subfamily *Opuntioideae* [12, 13]. OFI thrives in arid and semiarid regions and is cultivated for fruit production on approximately 100,000 hectares, mostly in semiarid areas across both hemispheres [14, 15]. The plant is rich in glucans, glycoproteins, and polysaccharides. Its high molecular weight fraction facilitates heavy metal retention primarily through complexation with carboxyl and hydroxyl functional groups. The polysaccharide fraction includes L-arabinose, D-galactose, L-rhamnose, D-xylose, and galacturonic acid [16]. Recent studies have shown that OFI is effective in removing heavy metals from contaminated water. For example, Barbera et al. [16] reported removal rates of 82% for Cd(II), 98% for Ni(II), 82% for Cu(II), and 90% for Pb(II) after 30 min of contact at pH 4 using 10 g/L of OFI and 0.01 mmol of each metal ion in single-element systems. Figueirôa et al. [15] observed a 84.9% removal rate of trivalent chromium from leather industry effluents within 5 min. OFI has also demonstrated the ability to treat organic pollutants. Othmani et al. [17] reported 83% color removal of methylene blue (MB) and 63% of methyl orange (MO) using lyophilized OFI, and 68% for MB and 65% for MO with oven-dried OFI, with an initial dye concentration of 0.1 g/L and a coagulant dosage of 0.3 g/L.

In parallel, many studies have explored the use of chitosan and its composites for heavy metal removal. Chitosan is a bio-based adsorbent known for its biodegradability and health benefits, including antimicrobial properties, wound healing, and immune system support. It is obtained by deacetylating chitin, which is found in crustaceans like crabs and shrimp [18]. Chitosan possesses amino and hydroxyl groups with free electron pairs that enable coordination and formation of stable complexes with heavy metals [19]. Its adsorption capacity increases with a higher degree of deacetylation (DD), due to a greater number of amino groups [20]. The effectiveness of chitosan has been demonstrated in multiple studies. For instance, Xiao et al. [19] reported removal rates of 91.4% for Cr(III), 90.5% for Co(II), and 95.7% for Pb(II) using three chitosan-based bio-adsorbents. Similarly, Velasco-Garduño et al. [21] achieved a 99.0% removal of Cu(II) using a chitosan-based biodegradable biocomposite.

In the present study, the effectiveness of OFI, CS, and their composites (OFI/CS 1:1 and OFI/CS 1:2) in removing inorganic pollutants, specifically Pb(II), Ni(II), Cu(II), and Cd(II), from aqueous solutions was evaluated. The influence of various physicochemical parameters was examined, including contact time, adsorbent dosage, and pH. Several characterization techniques, including Fourier-Transform infrared spectroscopy (FTIR), scanning electron microscopy coupled with energy-dispersive X-ray spectroscopy (SEM/EDX), and elemental analysis, were employed to analyze the materials before and after adsorption. Finally, the bio-adsorption process was modeled using pseudo-first-order, pseudo-second-order, and Elovich kinetic models, as well as the Freundlich, Langmuir, and Dubinin–Radushkevich isotherm models.

2 Materials and Methods

2.1 Reagents and Solutions

All reagents that were used in this study are of analytical grade.

Chitosan ≥ 75% deacetylated, glacial acetic acid 99%, acetic acid 67–69%, sodium hydroxide, and hydrochloric acid 37–39% were purchased from Sigma-Aldrich. Nitric acid 68% was purchased from Fisher Scientific. Distilled water with conductivity approx. 2.3 µs/cm at 25 °C was obtained from GFL Gesellschaft Fuer Labortec™ 2008. Ultrapure water with a resistivity of 18.2 MΩ.cm was obtained from PURELAB flex 1 system.

The standards were prepared from nickel sulfate $NiSO_4$ and cadmium acetate $Cd(CH_3COO)_2$, both of which were purchased from NORMAPUR, lead nitrate $Pb(NO_3)_2$ from AnalytiCals, and copper nitrate $Cu(NO_3)_2$ from ACROS. The solutions were filtered with 0.45 µm nylon springer filters purchased from Fisher Scientific.

2.2 Preparation of Opuntia ficus-indica

The *Opuntia ficus-indica* cactus was collected in the Constantine region in the northeast of Algeria during the summer of 2023. The cactus cladodes were washed with tap water, in order to remove dirt and impurities. After the thorns were removed, the cladodes were cut into small pieces of 2–3 cm, washed carefully with distilled water, and then dried under sunlight (40–43 °C) for a month. The dried biomass was ground using a Proficook mixer (model PC-KSW 1021 N) and gradually sieved to obtain a powder of ≤ 100 µm.

2.3 Preparation of Composites from Opuntia ficus-indica and Chitosan

Two different proportions of composite were prepared, by association of OFI and Chitosan, 1:1 (m/m) and 1:2 (m/m). First, in the case of OFI/CS 1:1 (m/m), OFI (typically 5 g) was stirred in 10% acetic acid (250 mL) for 1 h, at 20 °C, and 100 rpm, on a hotplate & stirrer (LMS-1003, LabTech). Then the required mass of chitosan (typically 5 g) was added to the solution. The latter was left under stirring for 3 h, ensuring the completely dissolution of CS. The solution containing OFI and CS was transferred into 0.5 M NaOH (typically 500 mL) and left under stirring overnight, which leads to the formation of a gel. The composite was then separated from the gel by centrifugation at 8000 rpm for 7 min using SIGMA 2-16P universal centrifuge. Subsequently, the composite was rinsed a few times with small portions of distilled water until the rinsing water's pH settled within the range [6, 7]. Same thing for OFI/CS 1:2, except that the quantity of CS was double that of OFI.

2.4 Batch Adsorption Experiments

The adsorption of heavy metals (Cu(II), Ni(II), Cd(II), and Pb(II)) was carried out in a multi-heavy metals system at different conditions of initial concentration, adsorbent mass, and initial pH. The latter was varied from 4 to 6. The kinetics were monitored for 240 min, under continuous stirring at 30 rpm, at 20 °C, using a Fisher Scientific multi-purpose tube rotator. In all the essays, the initial metal concentration was set at some selected values, ranging from 1 to 100 mg/L, to which was added a varying mass of adsorbent. A series of adsorbent concentration was explored (0.5; 1; 2 and 5 g/L) in order to determine the optimal adsorbent concentration. All experiments were performed in duplicate, and the standard deviation was less than 4%. Removal percentage and adsorption capacity were determined by Eqs. (1) and (2), respectively:

$$R\% = \frac{C_i - C_e}{C_i} \times 100 \tag{1}$$

$$q = \frac{(C_i - C_e) \times V}{m} \tag{2}$$

where $\boldsymbol{R\%}$ is the removal percentage of a specified metal, $\boldsymbol{q}$ is the adsorption capacity of the adsorbent (mg/g) for this metal, $\boldsymbol{C_i}$ and $\boldsymbol{C_e}$ are the initial and equilibrium (at the test end) concentrations of this metal (mg/L), respectively, $\boldsymbol{V}$ is the solution volume (L), and $\boldsymbol{m}$ is the mass of the adsorbent (g).

2.5 Methods

2.5.1 Fourier-Transform Infrared Spectroscopy (FTIR)

The structural properties of the treated adsorbents (OFI, CS, and OFI/CS) were characterized by FTIR using a PerkinElmer spectrometer equipped with an attenuated total reflectance (ATR) accessory. Solid samples were placed directly onto the ATR crystal, ensuring optimal contact by applying light pressure to maximize signal transmission. Infrared spectra were recorded over the spectral range of 4000–600 cm^{-1} with a spectral resolution of 0.5 cm^{-1}. A background spectrum was acquired prior to each measurement to ensure rigorous baseline correction and minimize interferences. The obtained spectra were analyzed with the "PerkinElmer IR Spectrum software, Version 10.6.2" to identify characteristic functional groups and potential binding sites of the bio-adsorbents.

2.5.2 Scanning Electron Microscopy (SEM) coupled with Energy-Dispersive X-ray Spectroscopy (EDX)

The surface morphology and size distribution within the treated samples were characterized using SEM with a JCM-7000 (JEOL) instrument. The samples were stabilized on the sample holder using carbon tape, thereby enhancing conductivity and ensuring proper fixation during the analysis. Observations were conducted at an accelerating voltage of

5.0 kV, allowing for the capture of secondary electrons and backscattered electron images at various magnifications. The analysis of the obtained images was performed using the JEOL JCM-7000 software Version 3, facilitating the quantification of particle dimensions and morphology, as well as the assessment of the distribution of chemical components within the matrix through EDX.

2.5.3 Inductively Coupled Plasma-Atomic Emission Spectroscopy (ICP-AES)

After their desorption from the adsorbents samples surfaces used in the essays, the four metallic elements (Pb(II), Cu(II), Cd(II), and Ni(II)), were quantified using an iCAP 6300 Series ICP-AES (Thermo Fisher Scientific). Beforehand, the samples were subjected to digestion with nitric acid (HNO_3). The intensities of the emissions at the appropriate wavelengths of light were measured and the concentrations of the elements within the sample deduced. A calibration curve was worked out using a series of standard solutions for each metal. The quantification limits for Pb(II), Cu(II), Cd(II), and Ni(II) all the studied elements were estimated to be of the order of a few µg/L (part per billion, ppb). Data analysis was carried out by Thermo Scientific Qtegra software Version 2.10.4345.236.

2.6 Kinetic and Isotherm Models

2.6.1 Adsorption Kinetics' Modeling

In this study, the suitability of three kinetic models, the pseudo-first order (PFO), pseudo-second order (PSO), and Elovich, was evaluated to describe the adsorption kinetics and to better understand the rate-controlling steps and potential mechanisms involved in the adsorption of metal cations onto the adsorbent surface. In the following equations, i.e., from Eqs. 3 to 13, $\boldsymbol{q}$ stands for the metal adsorbed mass on a unit mass of adsorbent (i.e., the surface concentration, in mg/g) at contact time t ($\boldsymbol{q_t}$) or at equilibrium ($\boldsymbol{q_e}$). (**qm**) is the maximum amount of metal that can be adsorbed on the surface of a unit mass of adsorbent, forming a saturated monolayer (in mg/g).

The pseudo-first-order model, also known as the Lagergren first-order model, is expressed by the following integrated form (Eq. 3), in which k_1 is the first-order adsorption rate constant:

$$q_t = q_e[1 - \exp(-k_1 t)] \tag{3}$$

Its suitability was tested through its linear form (Eq. 4):

$$\ln(q_e - q_t) = \ln q_e - k_1 t \tag{4}$$

The pseudo-first-order kinetic model assumes that the rate of adsorption is mainly controlled by the diffusion of the adsorbate on the adsorbent surface [22], where the heavy metals interact with the adsorbent surface through physisorption, primarily driven by physical forces such as van der Waals forces or electrostatic interaction [23].

In its integral form, the equation of the pseudo-second-order model is given by (Eq. 5), where k_2 is the second-order adsorption rate constant:

$$\frac{1}{(q_e - q_t)} = \frac{1}{q_e} + k_2 t \tag{5}$$

and its equivalent linear form is given by (Eq. 6):

$$\frac{1}{q_t} = \frac{1}{q_e} + \frac{1}{k_2 q_e^2} \tag{6}$$

The model assumes that the adsorption rate of the adsorbate is directly proportional to the number of available sites on the adsorbent surface [24], and the interaction adsorbent–adsorbate is of chemical nature (chemisorption) [23].

The Elovich model helps to better understand the chemisorption nature of process [24]. Its integral form is (Eq. 7):

$$q_t = \frac{1}{\beta}\ln(\alpha\beta t + 1), \tag{7}$$

which linearizes to (Eq. 8):

$$q_t = \frac{1}{\alpha}\ln(\alpha\beta) + \frac{1}{\alpha}\ln t \tag{8}$$

α is the initial adsorption rate (mg/g.min) and β is a desorption constant, expressed in mg/g. β relates to the extent of surface coverage and chemisorption activation energy.

The Elovich model is useful for predicting mass and surface diffusion, as well as activation and deactivation energies. The model was initially developed to characterize the chemisorption kinetics of gases on a solid surface. At present, it is also applied to describe liquid-phase sorption on heterogeneous adsorbent surfaces, where desorption is minimal [25].

2.6.2 Adsorption Isotherm Modeling

Adsorption isotherms provide a useful description of some characteristics of the interface between heavy metals and bio-adsorbents [26]. An adsorption isotherm describes the relationship between the amount of adsorbate fixed on a solid surface and the concentration of the adsorbate in the liquid or gas phase, at a constant temperature. These models are essential for understanding the interaction mechanisms between

adsorbent and adsorbate, determining the maximum adsorption capacity, and designing adsorption systems in various industrial and environmental contexts [27, 28]. In this study, the suitability of three adsorption models (Freundlich, Langmuir, and Dubinin–Radushkevich) was examined.

In the following equations, i.e., from Eqs. 9 to 13, (C_e) stands for the equilibrium concentration (mg/L) of a definite metal.

The Freundlich model is described by (Eq. 9):

$$q_e = K_f C_e^{\frac{1}{n}}, \tag{9}$$

which linearizes to (Eq. 10):

$$\log q_e = \log K_f + \frac{1}{n}\log C_e, \tag{10}$$

where K_f [(mg/g).(L/mg)$^{1/n}$] and n are the Freundlich constants for a given adsorbent/adsorbate couple. The Freundlich isotherm describes the sorption of various compounds onto heterogeneous surfaces or surfaces with sites of differing affinities [29].

The Langmuir adsorption model is described by (Eq. 11):

$$q_e = \frac{q_m K_L C_e}{1 + K_L C_e} \tag{11}$$

where q_e is the equilibrium adsorption capacity (mg/g), $q_{m\,is}$ the maximum adsorption capacity (mg/g), K_L (L/mg) is the Langmuir model constant, and C_e is the heavy metals concentration at equilibrium (mg/L).

This model assumes the formation of a monolayer on a homogeneous surface, with identical and energetically equivalent adsorption sites, and no interaction between the adsorbates [30].

Dubinin–Radushkevich adsorption model is described by (Eq. 12):

$$q_e = q_m \exp\left(-K\left[RT\ln\left(1+\frac{1}{C_e}\right)\right]^2\right),\ q_e = q_m \exp(-K\varepsilon^2) \tag{12}$$

and its equivalent linear form (Eq. 13) is:

$$\ln q_e = \ln q_m - K\varepsilon^2 \tag{13}$$

where K is Dubinin–Radushkevich constant of free energy of adsorption (mol^2/kJ^2) and ε is Polanyi potential (kJ/mol). K and ε relate to the adsorbent/adsorbate couple under study.

The Dubinin–Radushkevich model applies to physical adsorption processes involving pore filling. This isotherm suggests that adsorption occurs through multilayer formation driven by van der Waals forces [31].

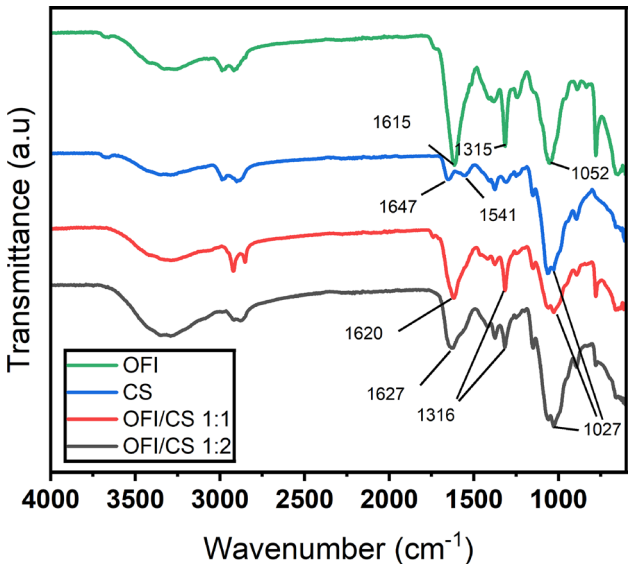


Fig. 1 FTIR spectrum of the absorbents OFI, Chitosan, OFI/CS 1:1, and OFI/CS 1:2

3 Results and Discussion

3.1 Adsorbent Characterization

3.1.1 FTIR Analysis

The FTIR spectrum of OFI powdered cladodes (Fig. 1) was recorded in the spectral range [4000–600] cm^{-1}. The band at 3264 cm^{-1} was attributed to the –OH stretching vibration of carboxylic acids [32]. Bands located between 3500 and 3200 cm^{-1} indicated the presence of amino groups in addition to carboxylic acids [33]. -OH and -NH groups are known to occur in the acidic and aliphatic components of cellulose as well as in aromatic proteins [34]. The peaks at 2988 cm^{-1} and 2917 cm^{-1} correspond to asymmetric –CH stretching vibrations [35]. The stretching vibration at 1614 cm^{-1} was associated with the C=O in carboxyl [33]. The intense band at 1051 cm^{-1} correspond to –CH–OH, indicative of the stretching in cyclic alcohols [36]. The bands at 778 cm^{-1} and 648 cm^{-1} correspond to the aromatic C=CH of phenols, as polyphenols occur in a high proportion in the structure of OFI and are believed to be responsible for the antioxidant properties of OFI [34]. The band at 1381 cm^{-1} was attributed to the stretching vibration of –COO [33]. The band at 1315 cm^{-1} showed the vibration of the –OH in phenols, and the peak at 1241 cm^{-1} was due to the presence of C–O stretching vibrations [32, 34].

The FTIR spectrum of chitosan, recorded between 4000 and 600 cm^{-1}, revealed a large band at 3290 cm^{-1}, representing a partial overlap of the stretching vibrations of the -OH and -NH groups. The two peaks at 2987 cm^{-1} and 2900 cm^{-1} were associated with symmetrical -CH stretching

[37]. At 1647 cm^{-1}, there was a notable C=O stretching band, characteristic of the acetyl group, alongside an -NH bending vibration within the amide group at 1551 cm^{-1}. The spectrum also displayed in-plane bending vibrations of $–CH_3$ at 1375.9 cm^{-1}, and a C–N stretching from the amide III at 1312 cm^{-1} [38]. Between 1065 and 1027 cm^{-1}, an intense band peaking at 1051 cm^{-1} was observed, mainly attributed to C–O stretching vibrations of acyclic alcohols or esters [37], with possible contributions from C–O–C linkages in the glycosidic bonds [39]. Peak observed at 1250 cm^{-1} was associated with the C-O stretching [39].

When comparing the OFI/CS 1:1 or OFI/CS 1:2 respective spectra to the OFI spectrum, manifest changes in bands intensities are observed. Both composites showed peak intensities in the 3700–3200 cm^{-1} range, associated with the –OH and –NH groups. In the OFI/CS 1:1 composite, the –CH stretching vibrations in the 3000–2800 cm^{-1} range were stronger, as indicated by the increased intensities of two peaks. Conversely, the OFI/CS 1:2 composite exhibited a single peak at 2878 cm^{-1} in this region. The spectral region from 1700 to 700 cm^{-1} displayed a combination of bands from both OFI and CS, with a noticeable difference in the 1650–1600 cm^{-1} range, indicative of C=O stretching. This peak was more intense in the OFI/CS 1:1 and OFI/CS 1:2 in comparison with CS, where its intensity is low. This increase in the intensity of the peak was due to the association with OFI, which shows a strong peak in this region. Additionally, there was a significant reduction in the intensity of the peak at 779 cm^{-1} in the OFI/CS 1:2 composite, typically linked to the = CH bond in polyphenol.

3.1.2 SEM–EDX and Elemental Analysis

The SEM micrographs at a 20 µm scale, corresponding to magnifications of × 3891 for OFI and × 3402 for chitosan (Fig. 2, decomposed into a and b), reveal significant morphological differences (in terms of shape and size) between the two materials. Figure 2a shows that the OFI surface exhibits an irregular texture with dispersed aggregates of varying sizes, shapes, and brightness, suggesting a rough and heterogeneous morphology. The bright particles, which appear more intense under backscattered electrons (BSE), commonly attributed to their higher atomic number elements, are generally associated to mineral content [40]. Some cavities between particles are also noticeable. In contrast, chitosan surface (Fig. 2b) displays a smoother, more lamellar structure. Its surface appears more structured and compact. Only a few particles can be observed, scattered across the surface, seemingly similar in nature to the bulk material. The pronounced surface roughness observed in OFI suggests a potentially higher specific surface area compared to the relatively smoother chitosan surface. The roughness may confer a higher adsorption capacity to OFI as well as that of the two composites, while its greater surface heterogeneity could promote more efficient adsorption kinetics.

The composites OFI/CS 1:1 (Fig. 2c) and OFI/CS 1:2 (Fig. 2d), displayed at a 30 µm scale with a magnification of × 3000, exhibit hybrid surface textures, combining the irregular structure of OFI with the smoother appearance characteristic of chitosan. Some moderate morphological differences can be observed between the two composites. The surface of the OFI/CS 1:1 composite appears relatively rougher and more heterogeneous compared to that of OFI/CS 1:2, which exhibits a slightly smoother texture. In the latter, chitosan seems to have formed a more continuous coating, leading to a more extensive encapsulation of the OFI particles. Additionally, both composite surfaces display a number of cracks and cavities, which could serve as diffusion pathways. These microstructural observations suggest that the incorporation of chitosan, to some depth, into the OFI matrix does not significantly modify the main morphological features of the original materials. Thus, the chemical treatment the two original materials have undergone appear to have preserved the native molecular structures of both OFI and chitosan within the composite framework.

The EDX-measured elemental contents reported in this work are calculated as averages from five selected nanoscopic spots within each material. These localized measurements may vary due to the intrinsic heterogeneity of the materials at the nanoscale. Nevertheless, the resulting average values are considered to represent a good estimate of the overall elemental composition of the materials, as supported by the total mass which is always close to 100%. The average values of the EDX-measured elemental contents are reported in Table 1. As expected, these localized measurements demonstrated the high mass proportions of carbon and oxygen in all four materials, making up jointly around 90% of the total mass in most cases, reflecting their cellulosic and polysaccharidic backbones. Despite being based on five different spots, the averaged values are considered reasonably close to the materials' overall composition. Nitrogen contents, ranging from *ca.* 1.90% to 11.2%, come behind those of C and O, forming a non-negligible fraction of the total. It also varies as expected along the series, CS being richer in N than OFI, owing to its amine functional groups. The composites show intermediate nitrogen contents between those of OFI and CS, which is a consistent observation. Calcium (18.7%) and magnesium (0.830%) appeared as macro-elements in OFI, confirming its mineral-rich nature. These values are higher or slightly above the typically reported intervals, *ca.* [1.0–4.9%] and [0.2–0.8%], respectively [41–43], but not uncommon, as contents much depend on growing conditions, in particular the level of mineral content in soil and other environmental factors. This highlights the mineral-rich nature of OFI in Constantine, Algeria, where it grows and from which it was harvested and the potential of this plant in human and/or

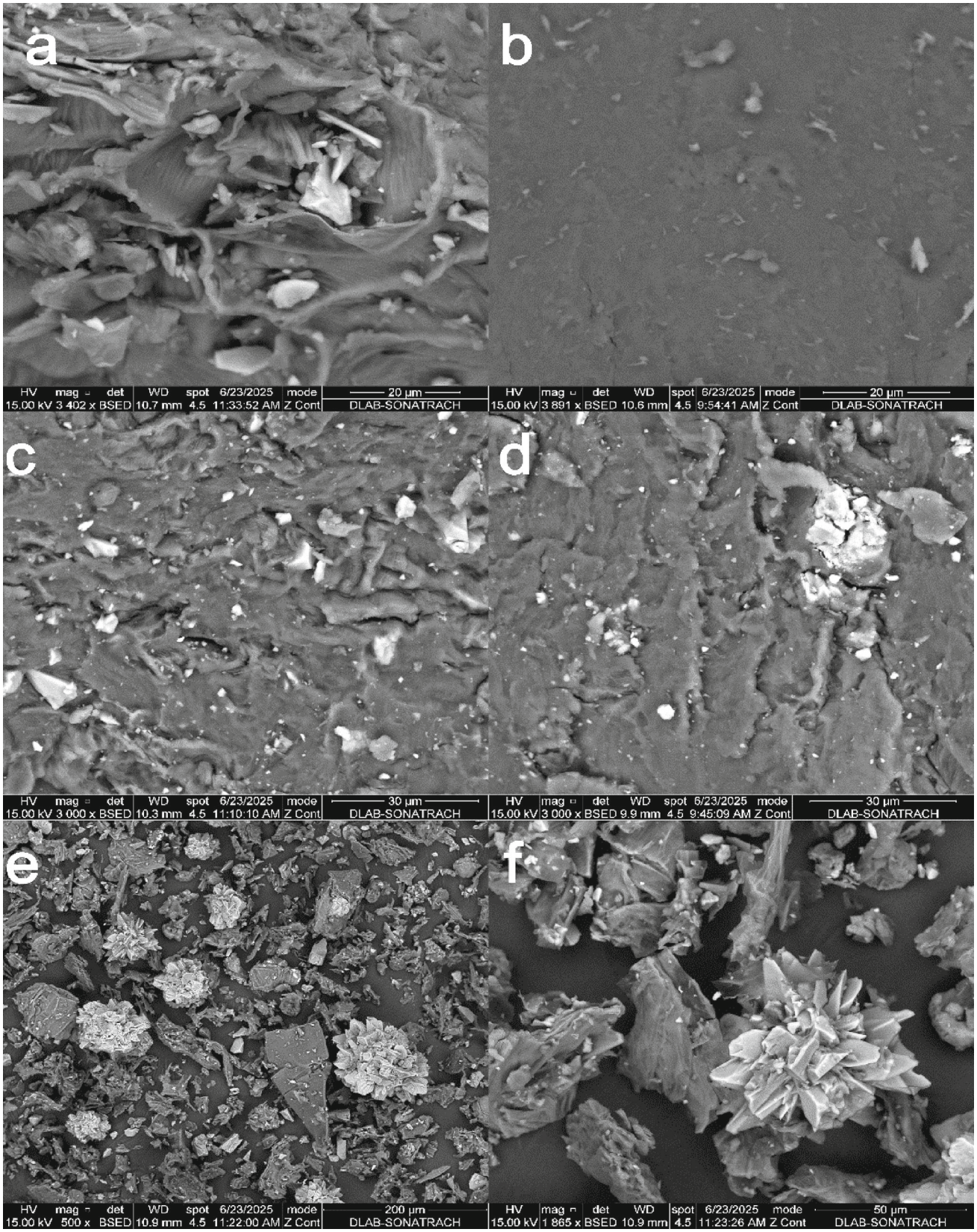


Fig. 2 Scanning electron microscopy (SEM) images of the adsorbents before adsorption. **a** OFI at a magnification of × 3891 (scale bar: 20 µm), **b** Chitosan at a magnification of × 3402 (scale bar: 20 µm), **c** OFI/CS 1:1 composite at a magnification of × 3000 (scale bar: 30 µm), **d** OFI/CS 1:2 composite at a magnification of × 3000 (scale bar: 30 µm), **e–f** High-magnification images showing the presence of calcium oxalate crystals on OFI surface with flower-like morphology

Table 1 EDX elemental analysis of adsorbents before adsorption, in mass percent

Bio-adsorbents	C (wt%)	O (wt%)	N (wt%)	Mg (wt%)	Ca (wt%)	Total mass (wt%)
OFI	30.6 ± 13	44.5 ± 12	1.93 ± 1.9	0.830 ± 0.85	18.7 ± 23	96.6
CS	43.2 ± 2.7	45.3 ± 1.9	11.2 ± 1.1	Not detected	Not detected	99.7
OFI/CS 1:1	40.4 ± 1.9	48.7 ± 2.4	5.48 ± 2.8	0.470 ± 0.21	4.58 ± 4.7	99.6
OFI/CS 1:2	41.9 ± 1.5	48.4 ± 1.5	8.43 ± 2.2	0.330 ± 0.27	0.900 ± 0.44	99.9

animal feeding. Calcium often accumulates in the form of microcrystals, commonly associated with oxalates or other counterions [44], which are observable by SEM/EDX. Similarly to what was observed for nitrogen, Ca, and Mg contents in the two composite materials are located between those of OFI (high amounts) and CS (negligible amounts).

These results underscore the structural and compositional improvements observed in the OFI/CS composites. The integration of chitosan into OFI increases its nitrogen content, while maintaining carbon and oxygen proportions within the same order of magnitude, thereby highlighting the availability of functional groups essential for adsorption processes.

After the adsorption process, for a practical reason, the EDX analysis focused on the OFI/CS 1:1 and OFI/CS 1:2 composites, as these materials demonstrated the most promising results in terms of heavy metal uptake efficiency. As shown in EDX spectrum (Fig. 3) and the corresponding data (not shown), the elemental compositions of the composites confirmed the presence of three (out of four) heavy metals, on the surface of one or the other bio-adsorbent, alongside the native elements mentioned above. Indeed, EDX confirmed the high mass proportions of carbon and oxygen and the presence of nitrogen. For both composites, EDX measurements showed that C, O, and N contents remained unchanged after carrying out the adsorption essays (variations of less than 1% in utmost cases, which fall within the experimental error margin), whereas Ca and Mg contents decreased. This suggests that the materials' original organic structures remained largely unchanged, as evidenced by the stable C, O, and N contents. The decrease in Ca observed during the composite preparation (Table 1) may be reasonably attributed to partial leaching induced by acetic acid and sodium hydroxide pretreatment which likely promoted the dissolution of Ca. The additional reduction of Ca and the complete disappearance of Mg (Table 2) during the adsorption stage is more plausibly ascribed to ion exchange between the residual mineral ions and heavy metals. [45].

It should be noted, as it is essential for the interpretation, that the elemental compositions discussed here are obtained from EDX analyses performed on five selected nanometric regions of each material's surface. For the OFI/CS 1:1 composite (Fig. 3a), Pb(II) dominates the spectrum, as indicated by the pronounced Pb-related peaks (PbMa, PbMb, PbLa, PbLb, PbLr), pointing to a strong Pb(II) adsorption. Cu(II) peaks (CuKa, CuKb, CuLa) are also evident, reflecting significant Cu(II) uptake, whereas Ni(II) appears in relatively lower intensities and peaks' number (NiKa, NiKb), and Cd(II) remains undetectable, indicating minimal or no adsorption. These data are coherent with the ICP-AES reported results, showing a marked affinity of the OFI/CS 1:1 material for Pb(II), followed by Cu(II), with much lower interaction with Ni(II) and Cd(II).

In contrast, the OFI/CS 1:2 composite (Fig. 3b) reveals an inverse trend regarding copper and lead, highlighting an enhanced Cu(II) adsorption. Lead remains present, as shown by distinct Pb(II) peaks, but with slightly less intense peaks than in the 1:1 composite. Nickel and cadmium peaks are absent, suggesting negligible adsorption. A competitive adsorption behavior seems at play, favoring Pb for the 1:1 composite, and Cu for the 1:2 composite. This differential uptake behavior, favoring Cu(II) and Pb(II), and near-excluding Ni(II) and Cd(II), further confirms the influence of the OFI-to-chitosan ratio on the material's metal ion preference.

On another note, significant variations in the measured concentrations of certain elements were observed across the five analyzed spots, as reflected by the high standard deviations, particularly for the mineral components (Ca and Mg) in OFI. This highlights the inherent heterogeneity of these natural biomaterials. This trend is consistently observed for all detected metals and both composite materials. Notably, Cu(II) reached a relatively high content of 22.6 ± 3% in one of the analyzed spots (data not shown), suggesting the presence of an "isolated" mass of cupper in this precise spot. It can be interpreted by the presence of a copper salt crystallite, on the surface of the organic matrix, in a manner similar to the natural formation of calcium oxalate on cladodes [46]. This hypothesis is supported by the SEM images (Fig. 2e and f), which clearly reveal the presence of calcium

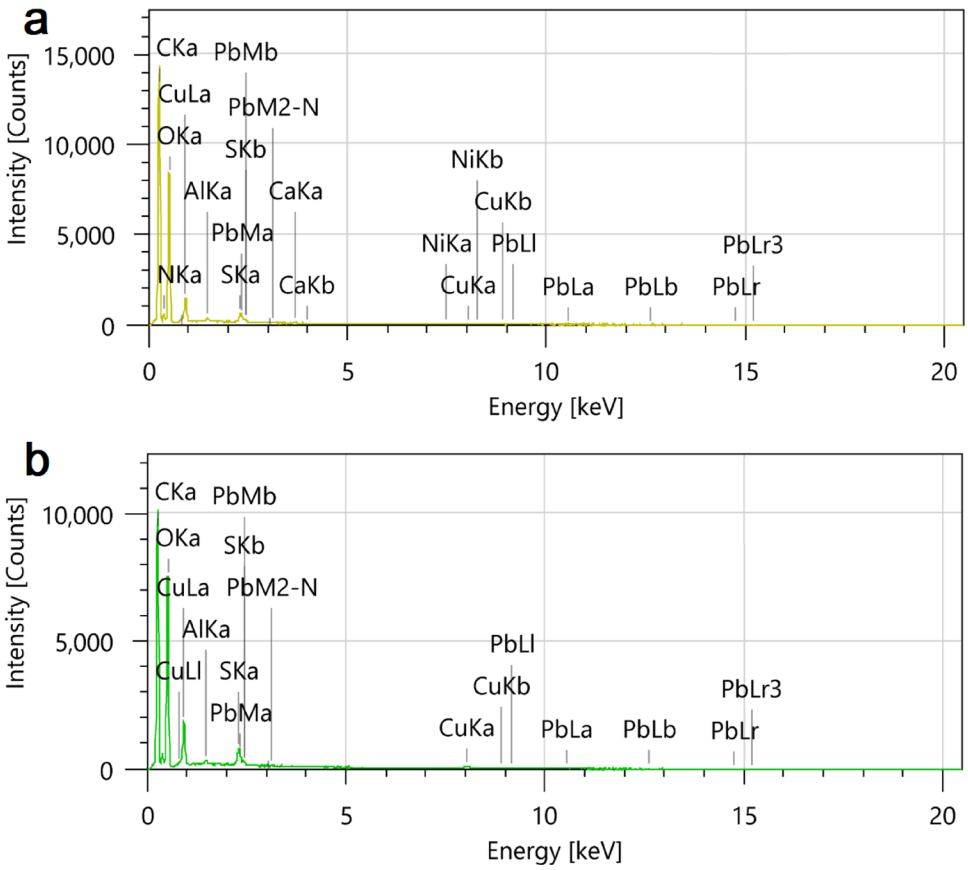


Fig. 3 EDX spectra of OFI/CS composites after heavy metals adsorption: **a** OFI/CS 1:1; **b** OFI/CS 1:2

Table 2 EDX elemental analysis of composites after adsorption, in mass percent

Bio-adsorbents	Mg (wt%)	Ca (wt%)
OFI/CS 1:1	Not detected	1.33 ± 2.6
OFI/CS 1:2	Not detected	0.270 ± 0.60

oxalate crystals exhibiting a characteristic flower-like morphology. These structures closely resemble those previously described by Contreras-Padilla et al. [44], who identified a variety of crystalline compounds naturally present in *Opuntia ficus-indica* cladodes, including calcium carbonate (calcite), calcium-magnesium bicarbonate, magnesium oxide, potassium peroxydiphosphate, potassium chloride, and notably calcium oxalate monohydrate. Our SEM findings align well with their observations, as the flower-like features detected on the OFI samples likely correspond to naturally occurring calcium oxalate deposits. This nano-heterogeneous distribution of adsorbed metals thus suggests that initial metal retention may take place at specific active sites, on which could subsequently grow crystallites of these very metals.

A much more accurate quantification of adsorbed heavy metals was carried out using inductively coupled plasma/atomic emission spectroscopy (ICP-AES). This technique was selected as the sole method for establishing the adsorption characteristics. The corresponding results are presented and discussed in detail in the following sections.

3.2 Effect of pH on Adsorption

The solution pH usually highly influences the adsorption amount of heavy metals in aqueous solutions. This study was conducted in an acidic environment (from pH 2 to 6) at constant temperature (20 °C), using an initial pollutant concentration of 50 mg/L, an adsorbent concentration of 0.5 g/L, and a contact time of 60 min. Before getting to the results, two facts must be mentioned: (i) In alkaline solutions, heavy metals precipitate by bonding to hydroxide ions, forming $Pb(OH)_2$, $Cd(OH)_2$, $Cu(OH)_2$, and $Ni(OH)_2$ precipitates [47, 48]; (ii) the same contact time was used for all experiments, corresponding to equilibrium conditions in most cases.

As shown in Fig. 4, the percent removal rates show varying profiles. Thus, no clear tendency emerges, when comparing the adsorption amount vs pH of the four elements onto the same material. This points to a potentially multifactorial influence. Nevertheless, some observations are worth mentioning. The adsorbed amounts (as a percent of the initial mass) are the lowest at pH = 2 for most cases, which may be

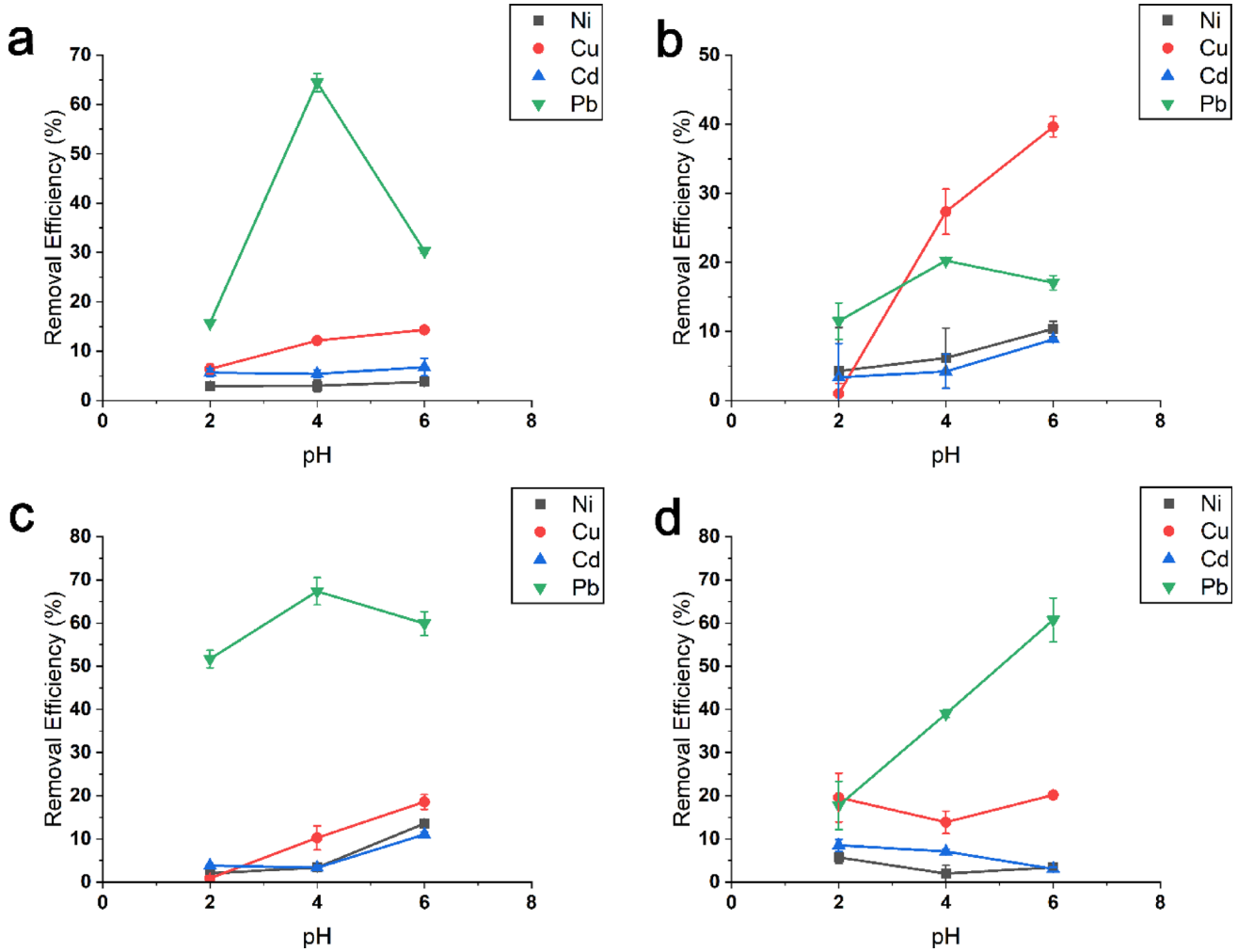


Fig. 4 Influence of pH on the Pb, Cu, Ni, and Cd removal efficiency (%), in multi-heavy metals system: **a** OFI, **b** Chitosan, **c** OFI/CS 1:1, **d** OFI/CS 1:2. Experimental conditions: adsorbent concentration = 0,5 g/L, $T = 20$ °C, $t = 60$ min, $C_0 = 50$ mg/L

attributed to a partial dissolution of CS, the dissolution being facilitated by the protonation of the amine groups in chitosan [49]. A most probable significant shift of the adsorption equilibrium toward the dissolved state may also contribute to this low performance. The adsorbed amounts increase when raising the pH to 4, sharply in some cases, only slightly in others, remaining, however, practically unchanged in a few cases. Disparate adsorption behaviors of the four elements are again observed when increasing the pH from 4 to 6. Indeed, some cases show improved percent adsorption amounts, while other cases exhibited no improvement or a little worsening amounts, for probably the same intricate and interdependent factors as between pH 2 and pH 4. On the whole, maximal removals of Cd(II), Ni(II), Cu(II) onto most adsorbents, and Pb(II) onto OFI/CS 1:2, were achieved at pH 6. Pb(II) is a notable exception, showing a clearly distinct behavior, with removal rates peaking at pH 4, onto CS as well as OFI or OFI/CS 1:1. A more precise interpretation requires consideration of the interconnected factors influencing the adsorption process: (i) Complexation of the metals to some surface groups acting as ligands, such as carboxylate, in those cases where metals' adsorption occurs by complexation [50]. This process is inhibited by the metals respective solubilities. Solubilization is indeed the reverse process of complexation, in an equilibrated reaction; (ii) affinity metal/adsorbent to form ion-pair, in those cases where metals' adsorption occurs by ionic bonds [51]. This, in itself, requires the acquisition of a negative charge of some surface groups which in fact is unlikely at low pHs; (iii) competition for adsorption sites, as the four metals fix most probably on the same sites, due to their similar nature (single divalent metal) [52]; and (iv) steric hindrance, for the narrowest pores [53], if any. In essence, this study brings about an approximate but useful trend to the influence of solution pH.

On a practical viewpoint, although none of the studied pHs shows maximal efficiency for all elements and all adsorbents,

pH 6 is nonetheless favorable for a short majority. As this pH falls within natural waters' pH range, treatment of the latter for the removal of heavy metals could therefore be accomplished without pH adjustment. pH 6 was adopted for the study of the potential influence of other physicochemical factors, aiming to replicate conditions as close as possible to those found in natural water systems.

3.3 Metal's Adsorption Temporal Evolution

To determine the time required to reach the equilibrium state (t_{eq}), the evolution of the amount (in percent of initial) of each metal adsorbed onto, respectively, OFI, chitosan, OFI/CS 1:1, or OFI/CS 1:2 was monitored as a function of contact time for 4–8 h.

For this purpose, an adsorbent concentration of 0.5 g/L, a pH of 6, and individual heavy metals concentrations of 50 mg/L were set as the initial conditions in multi-heavy metals system. For each essay, nine duplicate samples were collected at different contact times, starting from 1 min and ending at 240 min, and analyzed by ICP-AES. The obtained results are displayed in a graphical form in Fig. 5.

For practical purposes, Pb(II), Ni(II), and Cd(II), $\mathbf{t_{eq}}$ is reached in a very short time, ranging from 5 to 15 min. This remarkably swift adsorption points to a particularly high affinity of some adsorbent sites for heavy metals' cations. It is a promising indicator for the extraction of toxic metals from heavily polluted waters by non-expensive materials, in a simple process. Besides, these three metals exhibited almost parallel "percent removal versus time" profiles for the first two hours of reaction.

The initial uptake of Cu(II) is just as prompt as those of the other metals, followed by a plateau after *ca.* 15 min, at the exception of adsorption on CS where the levelling off starts at around 240 min. Therefore, the initial reaction rate of Cu(II) shows no significant difference compared to the other metals' reaction rates with the same adsorbent, respectively. However, at a later stage, i.e., after *ca.* 15 min, a second moderate rise of Cu(II) amount adsorbed on both composites is observed. This singular behavior may be attributed to a cation exchange between adsorbed Pb(II) and dissolved Cu(II), as the modest rise of Cu(II) uptake coincides with a small near-equivalent release of the adsorbed Pb(II).

For the sake of comparison, some studies have shown equilibrium times extending to several hours for the removal of similar heavy metals. For example, the equilibrium adsorptions of Pb(II), Cu(II), Ni(II), and Co(II) by high nitrogen activated carbon were achieved in around 10 h [54]. Pb(II), Cu(II), and Zn(II) were adsorbed by a tire-derived activated carbon and by a commercial activated carbon at equilibrium times of 6 h and 24 h, respectively [55]. Pb(II) and Cd(II) were adsorbed by cladodes of *Opuntia ficus-indica*, chemically modified with NaOH, with an optimal contact time of 2 h [11, 56]. At the other end of the spectrum, some studies showed much shorter adsorption equilibrium times, close to or slightly higher than those observed in this study. Thus, removal of Cr(III), Pb(II), and Cd(II) by sulfate aluminate cement–bentonite composites needed an optimal contact time of only 30 min.

3.4 Optimal Bio-adsorbent Dose

Figure 6 shows the effect of the initial bio-adsorbent concentration on the removal efficiency of each heavy metal, expressed in percent of the initial amount. Five concentrations (0.25, 0.5, 1, 2, and 5 g/L) were tested under the following conditions: initial pH of 6, a contact time of 180 min to ensure equilibrium was reached, and an initial concentration of 100 mg/L for each heavy metal.

As expected, in all cases, the removal efficiency increased with increasing adsorbent concentration. At low dosages, the amount of adsorbent was insufficient to effectively treat the relatively high pollutant load (a total initial concentration of 4 $\times$ 100 mg/L). As the bio-adsorbent concentration increased, the percentage of heavy metals removed rose with a decreasing slope, pointing to a lower efficiency. Up to a dose of 5 g/L, which is considered sufficiently high for practical applications, the removal efficiency continued to increase, although the slope of the curve levels off slightly at 2 g/L in a few cases. However, no inflection point nor plateauing were observed, and thus, no optimal dosage could be defined within the tested range. At 5 g/L, the composites already achieved very high removal efficiencies for lead and copper, reaching approximately 80% and 98%.

3.5 Comparison of the Materials' Adsorption Capacities and Metal Preferences

The histograms in Fig. 7 present the amounts of heavy metals removed, expressed as a percentage of the initial concentration, using an adsorbent dosage of 5 g/L. They are organized to illustrate the competitive adsorption among the four heavy metals on each adsorbent. From another perspective, the histograms also highlight the differences in adsorption efficiency among the four bio-adsorbents.

Several key observations can be drawn from Fig. 7:

- Among the original materials, OFI showed the highest removal efficiency for Pb(II), reaching 90.0%, while CS exhibited a clear preference for Cu(II), with a removal efficiency of 98.5%. The other two metals displayed moderate removal performances on both individual adsorbents.
- The fusion of CS and OFI significantly improved the adsorption of both Pb(II) and Cu(II), particularly on the OFI/CS 1:1 composite, which achieved removal efficiencies of 93.9% and 97.2%, respectively. The OFI/CS 1:2

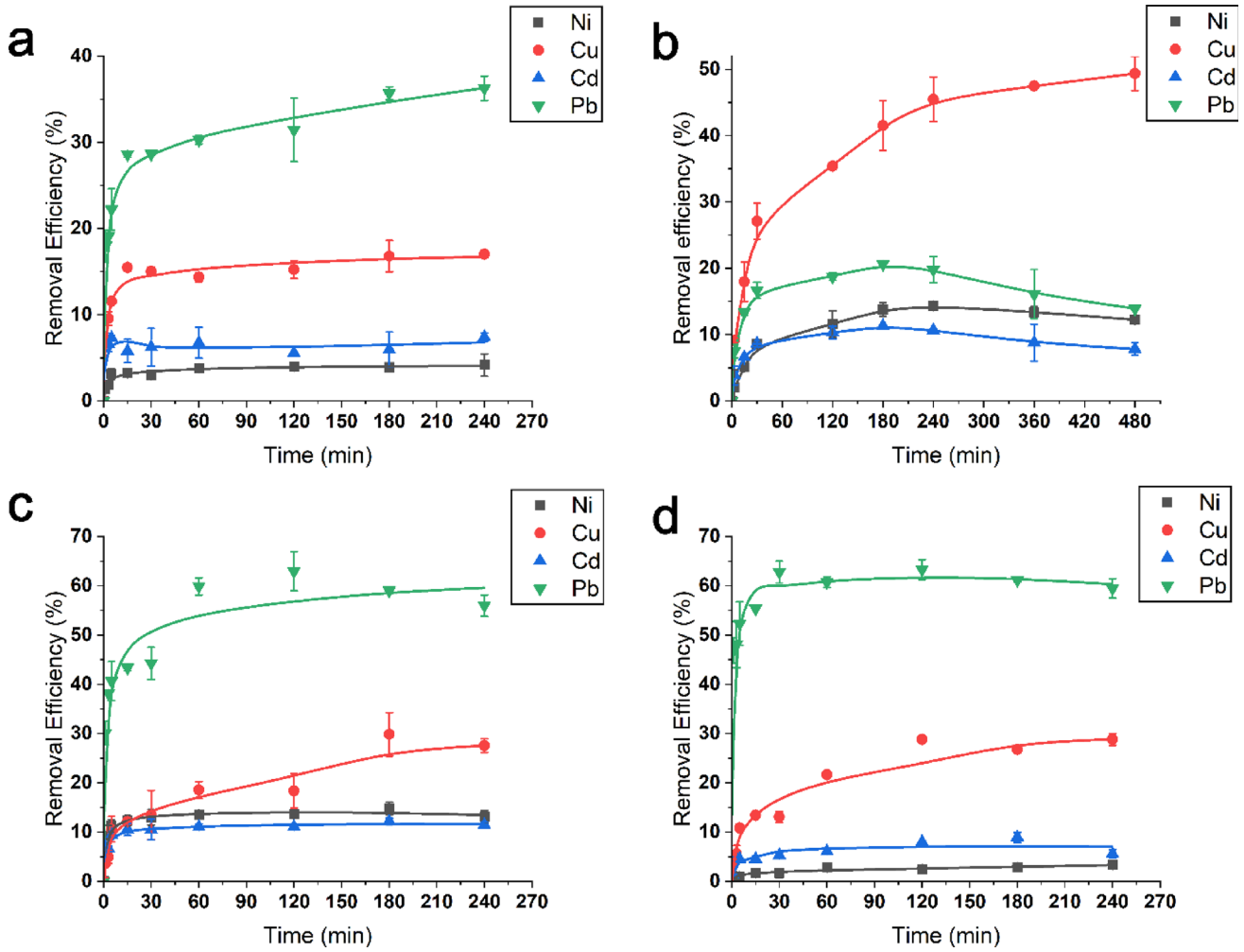


Fig. 5 Influence of contact time on, the mass percent removal amount in multi-heavy metals system: **a** OFI, **b** Chitosan, **c** OFI/CS 1:1, **d** OFI/CS 1:2. Experimental conditions: adsorbent concentration = 0.5 g/L, $T = 20$ °C, $C_0 = 50$ mg/L, pH = 6

composite also performed well, with 97.7% for Cu(II) and 81.6% for Pb(II). This synergistic enhancement, resulting from the merging of the two materials into a composite structure, represents one of the most significant achievement of this work. This improvement is primarily due to the complementary functional groups provided by both OFI and CS, such as hydroxyl (–OH), carboxyl (–COOH), amino ($–NH_2$), and carbonyl groups. Additionally, the well-preserved and relatively large surface area of OFI contributes to reinforcing this synergistic interaction.

According to Barbera et al. [57], OFI biomass contains galacturonic acid units with deprotonated carboxyl and amide groups capable of forming complexes with metal ions such as Pb(II) and Cu(II) through surface complexation. Similarly, chitosan is well known for its high density of amino groups, which bind strongly to Cu(II) via coordination bonds. Indeed, Chu [58] demonstrated that amine groups in partially deacetylated chitosan serve as primary coordination sites for Cu(II), enabling complex formation at near-neutral pH. The combination of OFI and CS thus broadens the variety, availability, and complementarity of active sites, enhancing both the adsorption capacity and versatility of the composite.

• In contrast, the individual adsorbents exhibited lower removal efficiencies for Cd(II) and Ni(II) (31.3% and 24.1% for OFI, and 26.7% and 32.2% for CS, respectively) compared to Pb(II) and Cu(II). The OFI/CS 1:1 composite led to a noticeable improvement (ca. 16% higher than the pure materials), whereas the 1:2 composite showed a slightly less pronounced enhancement. These results further suggest that although OFI and CS individually display some preference for one or the other metal, their fusion yields a more universal adsorbent with improved overall capacity.

- In terms of affinity, Pb(II) and Cu(II) were consistently the most effectively adsorbed ions. CS exhibited a strong preference for Cu(II), while OFI favored Pb(II). As previously discussed in Sect. 3.1 (Effect of pH), several

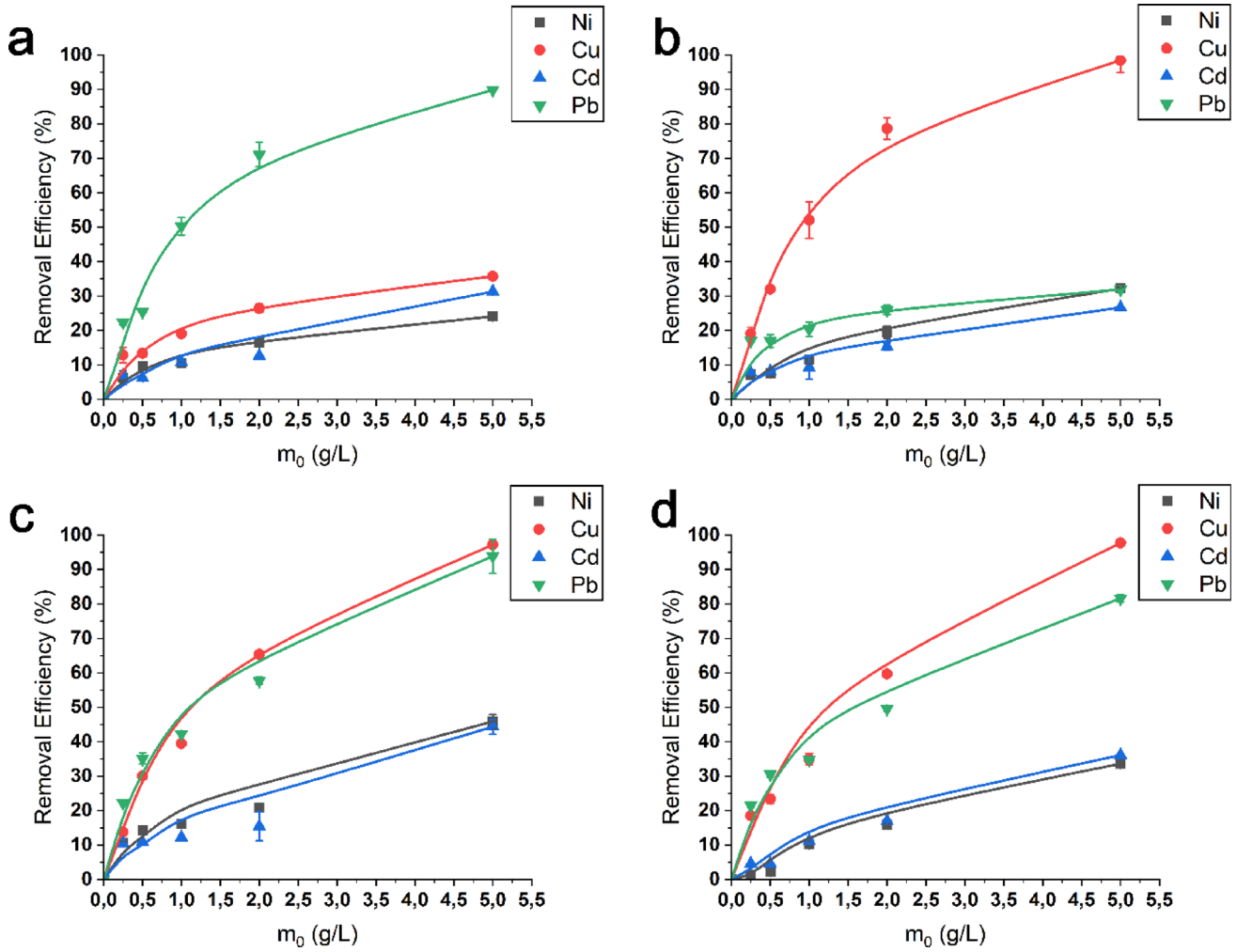


Fig. 6 Influence of the adsorbent mass on the removal efficiency (%), in multi-heavy metals system: **a** OFI, **b** Chitosan, **c** OFI/CS 1:1, **d** OFI/CS 1:2. Experimental conditions: $T = 20$ °C, $t = 180$ min, $C_0 = 100$ mg/L, pH = 6

factors influence adsorption behavior. However, it is reasonable to admit that the affinity between the adsorbent and the adsorbate is, all things considered, the main parameter governing the outcome of the adsorption competition among the four metallic cations. This affinity can, in turn, be attributed to the stability of the complex formed between the bio-adsorbent and the metal ion. Additionally, the strength of physical or physicochemical interactions should be considered.

Assuming that adsorption is a reversible process, as is typically observed in complexation reactions in aqueous solutions, differences in adsorption kinetics are not expected to play a major role, as rapid initial uptake may be followed by cations exchange at a later stage. A steric hindrance effect cannot be ruled out without dedicated experimental evidence. As to size competition, the ionic radii [∈ 69; 119 pm] of the four cations would likely allow them to penetrate any existing nanopores with roughly equal ease.

The competition for active sites can be attributed to the co-cation effect, affecting both adsorption thermodynamics and kinetics [59, 60]. This has been demonstrated in several studies, such as Kajeiou et al. [60], who observed competition between Zn(II), Cu(II), and Pb(II) on flax fibers, and Vievard et al. [23], who showed that competition is concentration-dependent. Lower removal efficiencies for Cd(II), Ni(II), and in some cases Cu(II) and Pb(II), may be attributed to the presence of acetate and sulfate counter ions, which compete with metal ions for active sites. The effect of counter ions depends on their type and concentration, playing a non-negligible role in determining the removal efficiency [61, 62].

- The presence of native copper in OFI is unlikely to significantly affect these results, as elemental analysis revealed

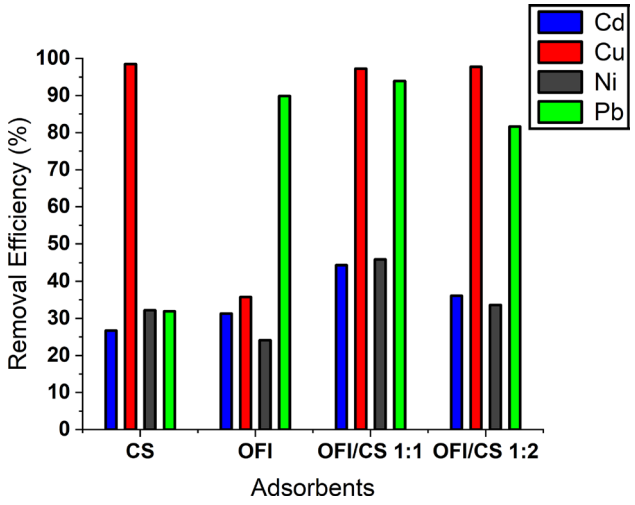


Fig. 7 Removal efficiency (%), at 180 min, in multi-heavy metals system: Experimental conditions: Adsorbent concentration = 5 g/L, T = 20 °C, Initial concentration of each metal = 100 mg/L, pH = 6

negligible levels, and reported values in the literature are low or non-existent (typically 0–2 ppm) [63].

3.6 Kinetic and Isotherm Studies

3.6.1 Kinetics

To get insight on the nature of the adsorption mechanism and the interaction tying the adsorbent and the adsorbate, three kinetic models were tested: pseudo-first order, pseudo-second order, and Elovich. Adsorption kinetics were recorded for 240 min for the bio-adsorbents OFI, OFI/CS 1:1, and OFI/CS 1:2, and for 480 min for chitosan, using an adsorbent concentration of 0.5 g/L and pollutants individual concentrations of 50 mg/L, in a multi-heavy metals system. Results of the adsorption kinetics modeling are displayed in Table 3, which gathers the models' characteristic constants, together with the values of the coefficients of determination of the non-linear fits (non-linear R^2).

As can be seen in Table 3, R^2 values vary on a broad scale, ranging virtually from zero to 1. Highly satisfactory values for the mechanism description are observed in many cases, such as Cd(II) on CS [R^2 (PSO) = 0.988], Cu(II) on CS [R^2 (Elovich) = 0.999], or Ni(II) on OFI/CS 1:2 [(R^2 Elovich = 0.982)].

Elovich model yielded generally higher coefficients of determination, reaching up to 0.999 and revealing that multilayer adsorption is taking place for these cases. Elovich model assumes that the rate of solute adsorption decreases exponentially as the amount of solute adsorbed increases [24]. This could explain the rapid initial adsorption of heavy metals on our bio-adsorbents within the first few minutes, followed by a gradual slowdown in adsorption rate over time.

In comparison, for a large majority of heavy metals and bio-adsorbents, PSO and PFO models exhibited lower R^2 values, in addition to being close, one relative to the other, and evolving likewise. In cases where R^2 values are high enough to validate these two models, it was deduced that chemisorption and physisorption phenomena are both involved in the adsorption processes, probably simultaneously for some systems. This point to the diversity and the complexity of the adsorption mechanisms involved, with possibly adsorption proceeding through more than one path in many cases. Nevertheless, the results are unable to assert if one of the paths is major or if the two paths are more or less balanced.

Besides, no general trend—that could account for a given metal's adsorption onto all adsorbents or for all metals adsorption onto a given material—emerges. Wide variations are sometimes observed when moving from one metal to the second on the same adsorbent or when moving from one adsorbent to the second for a given metal. For instance, all three models are well adapted for describing copper adsorption kinetics onto OFI/CS 1:1, with R^2 ranging from 0.991 to 0.994. On the opposite, none of the three models fits for the description of lead adsorption kinetics onto CS, with R^2 just reaching 0.0668 in the most favorable case.

3.6.2 Isotherms

The study of adsorption isotherms for the multi-heavy metals system was conducted using the classic Freundlich, Langmuir, and Dubinin–Radushkevich isotherm models. As a general observation, it can be stated that some adsorption systems are well described by a particular model, whereas other systems are best described by other models. The experiments were conducted at pH 6, with a contact time of 240 min, and a bio-adsorbent concentration of 0.5 g/L, while the initial heavy metal concentration varied from 1 to 100 mg/L. The characteristic constants and determination coefficients derived from the three studied models are reported in Table 4.

For the best-adsorbed metals, namely Pb(II) and Cu(II), the determination coefficients are high and mostly close to 1 across all three models and for all bio-adsorbents. Cu(II) in particular shows excellent fitting in the Langmuir model, with R^2 values reaching up to 0.995 and 0.997 for OFI and CS, respectively. Pb(II) also demonstrates high determination coefficients, particularly with the Langmuir model where the values reach 0.997, 0.997 and 0.994 for OFI, OFI/CS 1:1, and OFI/CS 1:2, respectively. For all bio-adsorbents, the adsorption behavior of nickel and cadmium was better described by the Freundlich and Dubinin–Radushkevich models, whereas the Langmuir model showed limited applicability in capturing their behavior across the studied materials. For Ni(II), the results are generally well suited by the two models except for

Table 3 PFO, PSO, and Elovich model parameter values for multi-heavy metals system

Heavy metals		PFO			PSO			Model Elovich		
		qe (mg/g)	k_1 (min^{-1})	R^2	qe (mg/g)	k_2 (g.min/mg)	R^2	α (mg/g.min)	β (g/mg)	R^2
OFI	Cd	5.83	518	0	5.83	1.89×10^{34}	0	7.48×10^{34}	18.6	0
	Cu	17.0	0.249	0.789	17.2	0.0286	0.897	229.9×10	0.761	0.946
	Ni	3.91	0.0612	0.573	4.17	0.0289	0.763	5.79	1.81	0.898
	Pb	29.3	0.366	0.562	31.3	0.0169	0.722	855	0.310	0.852
CS	Cd	10.8	0.0635	0.961	12.3	0.00624	0.988	2.98	0.466	0.928
	Cu	47.2	0.0127	0.965	53.7	3.44×10^{-4}	0.974	4.64	0.112	0.999
	Ni	14.1	0.0309	0.970	15.5	0.00244	0.945	1.33	0.348	0.882
	Pb	14.1	0.296	0.0668	14.1	0.0978	0.0233	1.62×10^{34}	7.66	0
OFI/CS 1:1	Cd	10.4	1.08	0.793	10.9	0.153	0.908	245.7×10	1.13	0.948
	Cu	25.6	0.0421	0.894	28.8	0.00169	0.948	2.89	0.177	0.981
	Ni	13.6	0.468	0.795	13.8	0.0655	0.938	290.7×10^2	1.11	0.776
	Pb	44.4	0.658	0.565	46.5	0.0315	0.660	158×10^2	0.248	0.908
OFI/CS 1:2	Cd	6.82	0.229	0.830	7.41	0.0373	0.875	5.37	0.828	0.872
	Cu	26.8	0.0785	0.991	28.4	0.00314	0.994	3.93	0.182	0.993
	Ni	1.73	0.655	0.760	1.90	0.355	0.829	3.28	2.95	0.982
	Pb	57.8	0.595	0.0981	61.0	0.0125	0.838	1.69×10^9	0.417	0.964

OFI/CS 1:2 in the Freundlich model, which displays a very low R^2 (0.0347). Cd(II), on the other hand, presents varying results: The fit is consistent and satisfactory for CS, OFI/CS 1:1, and OFI/CS 1:2 but very poor for OFI with Freundlich and Dubinin–Radushkevich.

Overall, the Freundlich and Langmuir models proved to be effective predictive tools for Pb(II) and Cu(II), while the adsorption of Ni(II) and Cd(II) was more accurately represented by the Freundlich and Dubinin–Radushkevich models.

Table 5 compares the maximum individual adsorption capacities (q_{max}) of Pb(II), Cu(II), Ni(II), and Cd(II) on our bio-adsorbents to other adsorbents' capacities reported in the literature. The experimental conditions for the multi-heavy metals system that yielded these results were as follows: pH = 6, $T = 20$ °C, $t = 240$ min, $C_0 = 100$ mg/L for each metal and $m_0 = 0.5$ g/L.

The maximum adsorption capacities of all metals show competitive or even higher performance in some cases. In particular, q_{max} for Pb(II) using OFI/CS 1:1 reaches 102 mg/g, which is higher than some reported values and comparable to others, as shown in Table 5. It is also worth noting that OFI/CS 1:1 exhibited higher maximum adsorption capacities than OFI alone for all the studied metals. Furthermore, the overall capacities of our materials, obtained by summing up the individual adsorbed amounts, showed that merging OFI and CS induced a notable improvement: 120 mg/g (OFI), 144 mg/g (CS), 183 mg/g (OFI/CS 1:1), 140 mg/g (OFI/CS 1:2).

In contrast, the maximum adsorption capacities for Ni(II) and Cd(II) were moderate compared to other bio-adsorbents. These outcomes can be attributed to the co-cation effect, i.e., the competition of heavy metals for adsorption sites.

It is noteworthy that literature values for the same adsorbate can vary significantly from one study to another. Such differences can be explained by the different physicochemical experimental conditions applied to obtain the results, such as pH, initial concentration of the adsorbate, initial concentration of the adsorbent, and whether the system is single- or multi-element.

4 Conclusion

This study aimed at determining the capacity of *Opuntia ficus-indica*, chitosan, and two composites made from these materials to retain heavy metal pollutants (Pb(II), Cu(II), Ni(II), and Cd(II)) in multi-heavy metals systems. The experimentally collected data enabled the determination of bio-adsorbents' efficiencies in removing each heavy metal and helped identify the most effective material for this application. The OFI/CS 1:1 composite stands out as the most efficient. Optimal physicochemical conditions, namely contact time, pH, and initial adsorbent concentration, were established. Adsorption phenomena were analyzed using kinetic models (PFO, PSO, and Elovich) and isotherm models (Langmuir, Freundlich, and Dubinin–Radushkevich). For Pb(II) and Cu(II), the Langmuir model provided the best

Table 4 Dubinin–Radushkevich models and Freundlich isotherm models parameter values for multi-heavy metals system

Bio-adsorbents	Heavy metals	Freundlich			Langmuir			Dubinin–Radushkevich		
		n	K_f (mg/g) (L/mg)$^{1/n}$	R^2	q_{max} (mg/g)	K_L (L/mg)	R^2	q_{max} (mg/g)	K (mol^2/kJ^2)	R^2
OFI	Cd	0.0751	1.79	0.0240	No relevant			20.0	1.35×10^3	0.657
	Cu	1.07	0.195	0.937	23.2	0.0258	0.995	No relevant		
	Ni	3.29	6.89×10^{-6}	0.956	No relevant			17.2	3.66×10^3	0.856
	Pb	1.49	0.478	0.954	59.5	0.291	0.997	No relevant		
CS	Cd	1.36	0.0358	0.967	No relevant			24.4	3.19×10^3	0.983
	Cu	0.354	13.9	0.979	56.7	0.214	0.997	No relevant		
	Ni	0.940	0.214	0.972	No relevant			18.0	1.85×10^3	0.953
	Pb	1.34	0.089	0.992	No relevant			44.6	2.36×10^3	0.958
OFI/CS 1:1	Cd	1.51	0.0145	0.954	No relevant			20.3	3.79×10^3	0.977
	Cu	0.494	4.03	0.917	34.7	0.0650	0.963	No relevant		
	Ni	2.12	9.43×10^{-4}	0.927	No relevant			26.0	5.58×10^3	0.957
	Pb	3.28	0.00138	0.938	102	0.0421	0.997	No relevant		
OFI/CS 1:2	Cd	0.908	0.136	0.857	No relevant			12.2	3.07×10^3	0.959
	Cu	0.357	9.82	0.983	46.9	0.140	0.970	No relevant		
	Ni	0.224	0.872	0.0347	No relevant			27.8	1.80×10^3	0.977
	Pb	1.25	0.477	0.973	53.4	0.0588	0.994	No relevant		

Table 5 Comparison of the maximum adsorption capacities (q_{max}) of heavy metals by different bio-adsorbents (mg/g)

Adsorbents	Pb(II)	Cu(II)	Ni(II)	Cd(II)	References
Cactus OFI	114	45.0	43.0	94.0	[16]
Chitosan	16.4	222	164	5.93	[64]
Fucus spiralis	141				[65]
Rice husk	108	29.0			[66]
Eichhornia crassipes	26.3–25.4			12.6–4.05	[67]
Phomopsis sp	179	25.0	6.00	26.0	[68]
Moringa oleifera tree leaves	209.55				[69]
Bacillus lentus		30.0		30.0	[70]
Banana peel	315				[71]
Olive cake	15.0				[72]
OFI	59.5	23.2	17.2	20.0	Present work
CS	44.6	56.7	18.0	24.4	Present work
OFI/CS 1:1	102	34.7	26.0	20.3	Present work
OFI/CS 1:2	53.4	46.9	27.8	12.2	Present work

fit, with very high determination coefficients ($R^2 = 0.997$), while the adsorption behaviors of Ni(II) and Cd(II) were better described by the Freundlich and Dubinin–Radushkevich models. When considering the adsorption of all four metals onto the same adsorbent, the Freundlich equation served as a slightly better global predictor, suggesting multilayer adsorption on heterogeneous surfaces. The OFI/CS 1:1 composite exhibited the highest total adsorption capacity, 183 mg/g, exceeding the capacities of OFI (120 mg/g) and CS (144 mg/g) individually. This highlights the synergistic effect of combining both materials. This study demonstrated that this bio-adsorbent exhibits retention values comparable to reported bio-adsorbents and, in some cases, showing superior potential. The following order of adsorption intensity was observed: Pb(II) > Cu(II) > Ni(II) ≈ Cd(II). This suggests that heavy metals compete for adsorption sites. Factors influencing this competition can be divided into intrinsic properties and external conditions setting. Hence, ease of complexation, solubility and crystal growth onto the surface are worth thorough investigation. Individual impact of pH, counterion, adsorbent and/or adsorbate concentrations, and more so their combined impact, may differ from one element to another. *Opuntia ficus-indica*, a key component of these bio-adsorbents, is abundantly available and is not actually being valorized. It can be cultivated in arid and semi-arid regions with minimal care, given its drought resistance and low water requirements. Its use without prior treatment makes it a low-cost and environmentally friendly option for heavy metal adsorption. This approach, which aims at valorizing waste materials as well as optimizing their efficiency, gave the most promising results. Consequently, further exploration of merging OFI with alternative materials of the same kind that could enhance its adsorption capacity and potentially expand its application to a broader range of pollutants, particularly toxic organics, is underway.

Acknowledgements This work has been partially supported by University of Rouen Normandy, INSA Rouen Normandy, the Centre National de la Recherche Scientifique (CNRS), European Regional Development Fund (ERDF) No. HN0001343, Labex SynOrg (ANR-11LABX-0029), Carnot Institute I2C, the graduate school for research XL-Chem (ANR-18-EURE-0020 XL CHEM), Region Normandie.

Author Contributions All authors contributed to the study's conception and design. Supervision and methodology were conducted by Slimane Kadouche, Juliette Vievard, and Mélanie Mignot. Abdelhamid Mili carried out conceptualization, investigation, and formal analysis and wrote the original draft, with Slimane Kadouche also contributing to conceptualization. Formal analysis was also performed by Juliette Vievard, Ferhat Mourad, Radia Tafer, Abdelaziz Boulkamh, and Slimane Kadouche. Christine Devouge-Boyer provided resources. Writing, review, and editing were undertaken by all authors. All authors read and approved the final manuscript.

Funding This research was funded by the Algerian Ministry of Higher Education and Scientific Research (Ministère Algérien de l'Enseignement Supérieur et de la Recherche Scientifique, MESRS) through the short-term mobility program abroad, as well as by University of Rouen Normandy, INSA Rouen Normandy, the Centre National de la Recherche Scientifique (CNRS), which provided additional financial support.

Data Availability The datasets used and/or analyzed during the current study are available from the corresponding author upon reasonable request.

Declarations

Conflict of interest The authors declare that they have no known competing financial interests or personal relationships that could have appeared to influence the work reported in this paper.

References

1. Choudhary, M.; Kumar, R.; Neogi, S.: Activated biochar derived from *Opuntia ficus-indica* for the efficient adsorption of malachite green dye, Cu+2 and Ni+2 from water. J. Hazard. Mater. **392**, 122441 (2020). https://doi.org/10.1016/j.jhazmat.2020.122441
2. Kobielska, P.A.; Howarth, A.J.; Farha, O.K.; Nayak, S.: Metal–organic frameworks for heavy metal removal from water. Coord. Chem. Rev. **358**, 92–107 (2018). https://doi.org/10.1016/j.ccr.2017.12.010
3. Alothman, Z.A.; Bahkali, A.H.; Khiyami, M.A.; Alfadul, S.M.; Wabaidur, S.M.; Alam, M.; Alfarhan, B.Z.: Low cost biosorbents from fungi for heavy metals removal from wastewater. Sep. Sci. Technol. **55**, 1766–1775 (2020). https://doi.org/10.1080/01496395.2019.1608242
4. Yang, X.; Liu, J.; McGrouther, K.; Huang, H.; Lu, K.; Guo, X.; He, L.; Lin, X.; Che, L.; Ye, Z.; Wang, H.: Effect of biochar on the extractability of heavy metals (Cd, Cu, Pb, and Zn) and enzyme activity in soil. Environ. Sci. Pollut. Res. **23**, 974–984 (2016). https://doi.org/10.1007/s11356-015-4233-0
5. Zhang, Y.; Ni, S.; Wang, X.; Zhang, W.; Lagerquist, L.; Qin, M.; Willför, S.; Xu, C.; Fatehi, P.: Ultrafast adsorption of heavy metal ions onto functionalized lignin-based hybrid magnetic nanoparticles. Chem. Eng. J. **372**, 82–91 (2019). https://doi.org/10.1016/j.cej.2019.04.111
6. Mubashar, M.; Naveed, M.; Mustafa, A.; Ashraf, S.; Shehzad Baig, K.; Alamri, S.; Siddiqui, M.H.; Zabochnicka-Świątek, M.; Szota, M.; Kalaji, H.M.: Experimental investigation of *Chlorella vulgaris* and *Enterobacter* sp. MN17 for decolorization and removal of heavy metals from textile wastewater. Water **12**, 3034 (2020). https://doi.org/10.3390/w12113034
7. Wang, Y.; Liu, Y.; Zhan, W.; Zheng, K.; Wang, J.; Zhang, C.; Chen, R.: Stabilization of heavy metal-contaminated soils by biochar: challenges and recommendations. Sci. Total. Environ. **729**, 139060 (2020). https://doi.org/10.1016/j.scitotenv.2020.139060
8. Punia, P.; Bharti, M.K.; Dhar, R.; Thakur, P.; Thakur, A.: Recent advances in detection and removal of heavy metals from contaminated water. ChemBioEng. Rev. **9**, 351–369 (2022). https://doi.org/10.1002/cben.202100053
9. Ahmed, S.F.; Kumar, P.S.; Rozbu, M.R.; Chowdhury, A.T.; Nuzhat, S.; Rafa, N.; Mahlia, T.M.I.; Ong, H.C.; Mofijur, M.: Heavy metal toxicity, sources, and remediation techniques for contaminated water and soil. Environ. Technol. Innov. **25**, 102114 (2022). https://doi.org/10.1016/j.eti.2021.102114
10. Solayman, H.M.; Hossen, M.A.; Abd Aziz, A.; Yahya, N.Y.; Leong, K.H.; Sim, L.C.; Monir, M.U.; Zoh, K.-D.: Performance evaluation of dye wastewater treatment technologies: a review. J. Environ. Chem. Eng. **11**, 109610 (2023). https://doi.org/10.1016/j.jece.2023.109610
11. Lavado-Meza, C.; Fernandez-Pezua, M.C.; Gamarra-Gómez, F.; Sacari-Sacari, E.; Angeles-Suazo, J.; Dávalos-Prado, J.Z.: Single and binary removals of Pb(II) and Cd(II) with chemically modified *Opuntia ficus indica* cladodes. Molecules **28**, 4451 (2023). https://doi.org/10.3390/molecules28114451
12. Kadda, S.; Belabed, A.; Conte, R.; Ouahhoud, S.; Hamdaoui, H.; Mechchate, H.; Elarbi, Z.: Phytochemical analysis for the residues of *Opuntia ficus indica* L seed oil of eastern region of Morocco. Mater. Today Proc. **72**, 3662–3668 (2023). https://doi.org/10.1016/j.matpr.2022.08.533
13. Plant breeding reviews, vol. 20. John Wiley & Sons, New York (2001)
14. Liguori, G.; Gaglio, R.; Greco, G.; Gentile, C.; Settanni, L.; Inglese, P.: Effect of *Opuntia ficus-indica* mucilage edible coating on quality, nutraceutical, and sensorial parameters of minimally processed cactus pear fruits. Agron. **11**, 1963 (2021). https://doi.org/10.3390/agronomy11101963
15. Figueirôa, J.A.; Menezes Novaes, G.U.; De Souza Gomes, H.; De Morais Silva, V.L.M.; De Moraes Lucena, D.; Lima, L.M.R.; De Souza, S.A.; Viana, L.G.F.C.; Rolim, L.A.; Da Silva Almeida, J.R.G.; Oliveira, A.P.D.; Gomes, J.P.: *Opuntia ficus-indica* is an excellent eco-friendly biosorbent for the removal of chromium in leather industry effluents. Heliyon **7**, e07292 (2021). https://doi.org/10.1016/j.heliyon.2021.e07292
16. Barbera, M.; Indelicato, S.; Bongiorno, D.; Censi, V.; Saiano, F.; Piazzese, D.: Untreated *Opuntia ficus indica* for the efficient adsorption of Ni(II), Pb(II), Cu(II) and Cd(II) ions from water. Molecules **28**, 3953 (2023). https://doi.org/10.3390/molecules28093953
17. Othmani, B.; Gamelas, J.A.F.; Rasteiro, M.G.; Khadhraoui, M.: Characterization of two cactus formulation-based flocculants and investigation on their flocculating ability for cationic and anionic dyes removal. Polymers **12**, 1964 (2020). https://doi.org/10.3390/polym12091964
18. Rahaman, M.H.; Islam, M.A.; Islam, M.M.; Rahman, M.A.; Alam, S.M.N.: Biodegradable composite adsorbent of modified cellulose and chitosan to remove heavy metal ions from aqueous solution. Curr. Res. Green Sustain. Chem. **4**, 100119 (2021). https://doi.org/10.1016/j.crgsc.2021.100119
19. Xiao, X.; Yu, Y.; Sun, Y.; Zheng, X.; Chen, A.: Heavy metal removal from aqueous solutions by chitosan-based magnetic composite flocculants. J. Environ. Sci. **108**, 22–32 (2021). https://doi.org/10.1016/j.jes.2021.02.014
20. Vakili, M.; Rafatullah, M.; Salamatinia, B.; Abdullah, A.Z.; Ibrahim, M.H.; Tan, K.B.; Gholami, Z.; Amouzgar, P.: Application of chitosan and its derivatives as adsorbents for dye removal from water and wastewater: a review. Carbohydr. Polym. **113**, 115–130 (2014). https://doi.org/10.1016/j.carbpol.2014.07.007
21. Velasco-Garduño, O.; Martínez, M.E.; Gimeno, M.; Tecante, A.; Beristain-Cardoso, R.; Shirai, K.: Copper removal from wastewater by a chitosan-based biodegradable composite. Environ. Sci. Pollut. Res. **27**, 28527–28535 (2020). https://doi.org/10.1007/s11356-019-07560-2
22. Wang, T.; Jiang, M.; Yu, X.; Niu, N.; Chen, L.: Application of lignin adsorbent in wastewater treatment: a review. Sep. Purif. Technol. **302**, 122116 (2022). https://doi.org/10.1016/j.seppur.2022.122116
23. Vievard, J.; Alem, A.; Pantet, A.; Ahfir, N.-D.; Leveneur, S.; Devouge-Boyer, C.; Daïch, E.; Mignot, M.: Competitive and non-competitive adsorption of six heavy metals on flax fibers. Emergent Mater. (2024). https://doi.org/10.1007/s42247-024-00648-7
24. William Kajjumba, G.; Emik, S.; Öngen, A.; Kurtulus Özcan, H.; Aydın, S.: Modelling of adsorption kinetic processes—errors, theory and application. In: Edebali, S. (Ed.) Advanced Sorption Process Applications. IntechOpen (2019)
25. Ugwu, E.I.; Othmani, A.; Nnaji, C.C.: A review on zeolites as cost-effective adsorbents for removal of heavy metals from aqueous environment. Int. J. Environ. Sci. Technol. **19**, 8061–8084 (2022). https://doi.org/10.1007/s13762-021-03560-3
26. Al-Zahrani, F.A.M.; Al-Shehri, B.M.; El-Shishtawy, R.M.: Removal of dye from aqueous solution using ectodermis of prickly pear fruits-based bioadsorbent. Sustainability **15**, 4700 (2023). https://doi.org/10.3390/su15064700
27. Wang, J.; Guo, X.: Adsorption isotherm models: classification, physical meaning, application and solving method. Chemosphere **258**, 127279 (2020). https://doi.org/10.1016/j.chemosphere.2020.127279
28. Al-Ghouti, M.A.; Daana, D.A.: Guidelines for the use and interpretation of adsorption isotherm models: A review. J. Hazard. Mater. **393**, 122383 (2020). https://doi.org/10.1016/j.jhazmat.2020.122383

29. Vilardi, G.; Di Palma, L.; Verdone, N.: Heavy metals adsorption by banana peels micro-powder: equilibrium modeling by non-linear models. Chin. J. Chem. Eng. **26**, 455–464 (2018). https://doi.org/10.1016/j.cjche.2017.06.026
30. Amrutha, J.G.; Girish, C.R.; Prabhu, B.; Mayer, K.: Multi-component adsorption isotherms review and modeling studies. Environ. Process. **10**, 38 (2023). https://doi.org/10.1007/s40710-023-00631-0
31. Boulaiche, W.; Hamdi, B.; Trari, M.: Removal of heavy metals by chitin: equilibrium, kinetic and thermodynamic studies. Appl Water Sci **9**, 39 (2019). https://doi.org/10.1007/s13201-019-0926-8
32. Louati, I.; Fersi, M.; Hadrich, B.; Ghariani, B.; Nasri, M.; Mechichi, T.: Prickly pear cactus cladodes powder of *Opuntia ficus indica* as a cost effective biosorbent for dyes removal from aqueous solutions. 3 Biotech **8**, 478 (2018). https://doi.org/10.1007/s13205-018-1499-1
33. Barka, N.; Abdennouri, M.; El Makhfouk, M.; Qourzal, S.: Biosorption characteristics of cadmium and lead onto eco-friendly dried cactus (*Opuntia ficus indica*) cladodes. J. Environ. Chem. Eng. **1**, 144–149 (2013). https://doi.org/10.1016/j.jece.2013.04.008
34. Oudir, M.; Ait Mesbah, Z.; Lerari, D.; Issad, N.; Djenane, D.: Development of eco-friendly biocomposite films based on *Opuntia ficus-indica* cladodes powder blended with gum arabic and xanthan envisaging food packaging applications. Foods. **13**, 78 (2023). https://doi.org/10.3390/foods13010078
35. Adjeroud-Abdellatif, N.; Hammoui, Y.; Boudria, A.; Agab, S.; Choulak, F.; Leclerc, J.-P.; Merzouk, B.; Madani, K.: Effect of a natural coagulant extract from *Opuntia ficus-indica* cladode on electrocoagulation-electroflotation water treatment process. Int. J. Environ. Anal. Chem. **102**, 5822–5846 (2022). https://doi.org/10.1080/03067319.2020.1804889
36. Vargas-Solano, S.V.; Rodríguez-González, F.; Martínez-Velarde, R.; Morales-García, S.S.; Jonathan, M.P.: Removal of heavy metals present in water from the Yautepec River Morelos México, using *Opuntia ficus-indica* mucilage. Environ. Adv. **7**, 100160 (2022). https://doi.org/10.1016/j.envadv.2021.100160
37. Medha, S.S.: RSM optimized chitosan based composite hydrogel for sustained drug delivery applications. Mater. Today Commun. **38**, 108029 (2024). https://doi.org/10.1016/j.mtcomm.2024.108029
38. Barbosa, H.F.G.; Francisco, D.S.; Ferreira, A.P.G.; Cavalheiro, É.T.G.: A new look towards the thermal decomposition of chitins and chitosans with different degrees of deacetylation by coupled TG-FTIR. Carbohydr. Polym. **225**, 115232 (2019). https://doi.org/10.1016/j.carbpol.2019.115232
39. Pawlak, A.; Mucha, M.: Thermogravimetric and FTIR studies of chitosan blends. Thermochim. Acta **396**, 153–166 (2003). https://doi.org/10.1016/S0040-6031(02)00523-3
40. Ali, A.; Zhang, N.; Santos, R.M.: Mineral characterization using scanning electron microscopy (SEM): a review of the fundamentals, advancements, and research directions. Appl. Sci. **13**(23), 12600 (2023). https://doi.org/10.3390/app132312600
41. Cheikh Rouhou, M.; Abdelmoumen, S.; Thomas, S.; Attia, H.; Ghorbel, D.: Use of green chemistry methods in the extraction of dietary fibers from cactus rackets (*Opuntia ficus indica*): structural and microstructural studies. Int. J. Biol. Macromol. **116**, 901–910 (2018). https://doi.org/10.1016/j.ijbiomac.2018.05.090
42. Procacci, S.; Bojórquez-Quintal, E.; Platamone, G.; Maccioni, O.; Vecchio, V.L.; Morreale, V.; Alisi, C.; Balducchi, R.; Bacchetta, L.: *Opuntia ficus-indica* pruning waste recycling: recovery and characterization of mucilage from cladodes. Nat. Resour. **12**, 91–107 (2021). https://doi.org/10.4236/nr.2021.124008
43. Rivera Cañón, A.F.; Hernández Carrillo, C.G.; Gómez Cuaspud, J.A.: Evaluation of physicochemical properties of Nopal (*Opuntia ficus-indica*) as bio coagulant-flocculant for water treatment. J. Phys. Conf. Ser. **2046**, 012057 (2021). https://doi.org/10.1088/1742-6596/2046/1/012057
44. Contreras-Padilla, M.; Rivera-Muñoz, E.M.; Gutiérrez-Cortez, E.; Del López, A.R.; Rodríguez-García, M.E.: Characterization of crystalline structures in *Opuntia ficus-indica*. J. Biol. Phys. **41**, 99–112 (2015). https://doi.org/10.1007/s10867-014-9368-6
45. Tejada-Tov, C.: Effect of the adsorbent dose and initial cConOtNamTEinNaInDt Oconcentration on the removal of VoluPmben(I8I,)niúnmaersoo3lu, 2ti0o0n9 /uVsoinlugmOe p8,unnutmiabfiercu3,s2I0n0d9ica shell Efecto de la dosis de adsorbente y concentración inicial en la remoción de Pb(II) usando cáscara de Opuntia ficus Indica. **20**, (2021)
46. Rojas-Molina, I.; Gutiérrez-Cortez, E.; Bah, M.; Rojas-Molina, A.; Ibarra-Alvarado, C.; Rivera-Muñoz, E.; Del Real, A.; Aguilera-Barreiro, M.D.L.A.: Characterization of calcium compounds in *Opuntia ficus indica* as a source of calcium for human diet. J. Chem. **2015**, 1–8 (2015). https://doi.org/10.1155/2015/710328
47. Tünay, O.; Kabdaşli, N.I.: Hydroxide precipitation of complexed metals. Water Res. **28**, 2117–2124 (1994). https://doi.org/10.1016/0043-1354(94)90022-1
48. Pang, F.M.; Teng, S.P.; Teng, T.T.; Omar, A.K.M.: Heavy metals removal by hydroxide precipitation and coagulation-flocculation methods from aqueous solutions. Water Qual. Res. J. **44**, 174–182 (2009). https://doi.org/10.2166/wqrj.2009.019
49. Sogias, I.A.; Khutoryanskiy, V.V.; Williams, A.C.: Exploring the factors affecting the solubility of chitosan in water. Macromol. Chem. Phys. **211**, 426–433 (2010). https://doi.org/10.1002/macp.200900385
50. Hocking, R.K.; Hambley, T.W.: Structural measure of metal−ligand covalency from the bonding in carboxylate ligands. Inorg. Chem. **42**, 2833–2835 (2003). https://doi.org/10.1021/ic034198a
51. Tian, M.; Fang, L.; Yan, X.; Xiao, W.; Row, K.H.: Determination of heavy metal ions and organic pollutants in water samples using ionic liquids and ionic liquid-modified sorbents. J. Anal. Methods Chem. **2019**, 1–19 (2019). https://doi.org/10.1155/2019/1948965
52. Srivastava, P.; Singh, B.; Angove, M.: Competitive adsorption behavior of heavy metals on kaolinite. J. Colloid Interface Sci. **290**, 28–38 (2005). https://doi.org/10.1016/j.jcis.2005.04.036
53. Guo, X.; Zhao, B.; Wang, L.; Zhang, Z.; Li, J.: Asymmetrically charged polyamide nanofilm of intrinsic microporosity containing quaternary ammonium groups for heavy metal removal. J. Membr. Sci. **698**, 122620 (2024). https://doi.org/10.1016/j.memsci.2024.122620
54. Yuan, Y.; An, Z.; Zhang, R.; Wei, X.; Lai, B.: Efficiencies and mechanisms of heavy metals adsorption on waste leather-derived high-nitrogen activated carbon. J. Clean. Prod. **293**, 126215 (2021). https://doi.org/10.1016/j.jclepro.2021.126215
55. Shahrokhi-Shahraki, R.; Benally, C.; El-Din, M.G.; Park, J.: High efficiency removal of heavy metals using tire-derived activated carbon vs commercial activated carbon: insights into the adsorption mechanisms. Chemosphere **264**, 128455 (2021). https://doi.org/10.1016/j.chemosphere.2020.128455
56. Niu, M.; Li, G.; Cao, L.; Wang, X.; Wang, W.: Preparation of sulphate aluminate cement amended bentonite and its use in heavy metal adsorption. J. Clean. Prod. **256**, 120700 (2020). https://doi.org/10.1016/j.jclepro.2020.120700
57. Barbera et al. (2023) Untreated Opuntia ficus indica for the Efficient A.pdf
58. Chu, K.: Removal of copper from aqueous solution by chitosan in prawn shell: adsorption equilibrium and kinetics. J. Hazard. Mater. **90**, 77–95 (2002). https://doi.org/10.1016/S0304-3894(01)00332-6
59. Puranik, P.R.; Paknikar, K.M.: Influence of co-cations on biosorption of lead and zinc – a comparative evaluation in binary and

multimetal systems. Bioresour. Technol. (1999). https://doi.org/10.1016/S0960-8524(99)00037-1
60. Jain, M.; Garg, V.K.; Kadirvelu, K.; Sillanpää, M.: Adsorption of heavy metals from multi-metal aqueous solution by sunflower plant biomass-based carbons. Int. J. Environ. Sci. Technol. **13**, 493–500 (2016). https://doi.org/10.1007/s13762-015-0855-5
61. Inglezakis, V.; Zorpas, A.; Loizidou, M.; Grigoropoulou, H.: The effect of competitive cations and anions on ion exchange of heavy metals. Sep. Purif. Technol. **46**, 202–207 (2005). https://doi.org/10.1016/j.seppur.2005.05.008
62. Sandoval-Flores, G.; Alvarado-Reyna, S.; Elvir-Padilla, L.G.; Mendoza-Castillo, D.I.; Reynel-Avila, H.E.; Bonilla-Petriciolet, A.: Kinetics, thermodynamics, and competitive adsorption of heavy metals from water using orange biomass. Water Environ. Res. **90**, 2114–2125 (2018). https://doi.org/10.2175/106143017X15131012188321
63. Nedjimi, B.: Determination of some major and trace elements in cladodes of Barbary fig (*Opuntia ficus-indica* Mill.) by X-ray fluorescence spectrometry. Biol. Trace Elem. Res. **199**, 4353–4359 (2021). https://doi.org/10.1007/s12011-020-02555-4
64. Babel, S.: Low-cost adsorbents for heavy metals uptake from contaminated water: a review. J. Hazard. Mater. **97**, 219–243 (2003). https://doi.org/10.1016/S0304-3894(02)00263-7
65. Filote, C.; Volf, I.; Santos, S.C.R.; Botelho, C.M.S.: Bioadsorptive removal of Pb(II) from aqueous solution by the biorefinery waste of *Fucus spiralis*. Sci. Total. Environ. **648**, 1201–1209 (2019). https://doi.org/10.1016/j.scitotenv.2018.08.210
66. Wong, K.K.; Lee, C.K.; Low, K.S.; Haron, M.J.: Removal of Cu and Pb by tartaric acid modified rice husk from aqueous solutions. Chemosphere **50**, 23–28 (2003). https://doi.org/10.1016/S0045-6535(02)00598-2
67. Mahamadi, C.; Nharingo, T.: Competitive adsorption of Pb2+, Cd2+ and Zn2+ ions onto *Eichhornia crassipes* in binary and ternary systems. Bioresour. Technol. **101**, 859–864 (2010). https://doi.org/10.1016/j.biortech.2009.08.097
68. Saiano, F.; Ciofalo, M.; Olga Cacciola, S.; Ramirez, S.: Metal ion adsorption by Phomopsis sp. biomaterial in laboratory experiments and real wastewater treatments. Water Res. **39**, 2273–2280 (2005). https://doi.org/10.1016/j.watres.2005.04.022
69. Reddy, D.H.K.; Harinath, Y.; Seshaiah, K.; Reddy, A.V.R.: Biosorption of Pb(II) from aqueous solutions using chemically modified *Moringa oleifera* tree leaves. Chem. Eng. J. **162**, 626–634 (2010). https://doi.org/10.1016/j.cej.2010.06.010
70. Vianna, L.N.L.; Andrade, M.C.; Nicoli, J.R.: Screening of waste biomass from *Saccharomyces cerevisiae*, *Aspergillus oryzae* and *Bacillus lentus* fermentations for removal of Cu, Zn and Cd by biosorption. World J. Microbiol. Biotechnol. **16**, 437–440 (2000). https://doi.org/10.1023/A:1008953922144
71. Zhou, N.; Chen, H.; Xi, J.; Yao, D.; Zhou, Z.; Tian, Y.; Lu, X.: Biochars with excellent Pb(II) adsorption property produced from fresh and dehydrated banana peels via hydrothermal carbonization. Bioresour. Technol. **232**, 204–210 (2017). https://doi.org/10.1016/j.biortech.2017.01.074
72. Blázquez, G.; Calero, M.; Ronda, A.; Tenorio, G.; Martín-Lara, M.A.: Study of kinetics in the biosorption of lead onto native and chemically treated olive stone. J. Ind. Eng. Chem. **20**, 2754–2760 (2014). https://doi.org/10.1016/j.jiec.2013.11.003

Springer Nature or its licensor (e.g. a society or other partner) holds exclusive rights to this article under a publishing agreement with the author(s) or other rightsholder(s); author self-archiving of the accepted manuscript version of this article is solely governed by the terms of such publishing agreement and applicable law.